International Journal of Non-Linear Mechanics 118 (2020) 103260

Contents lists available at ScienceDirect

International Journal of Non-Linear Mechanics

journal homepage: www.elsevier.com/locate/nlm

Fibrous soft tissues damage evaluation with a coupled thermo-visco-hyperelastic model

Arash Mohammadali Zadeh Fard, Farid Vakili-Tahami *

Department of Mechanical Engineering, University of Tabriz, Tabriz, Iran

ARTICLE INFO

Keywords:
Coupled thermo-mechanical analysis
Thermo-visco-hyperelasticity
Damage mechanics
Fibrous soft tissue
Temperature dependent properties

ABSTRACT

We model the thermo-visco-hyperelastic behavior of soft tissues using a thermodynamic framework. For this purpose, we develop a rheological model which can predict the stress–stretch behavior as well as the temperature variation due to visco-hyperelasticity and rate-dependent damage of the matrix and fibers. In a second stage, we carry out a set of cyclic uniaxial tensile tests to provide experimental data and calculate the material constants for the constitutive model utilizing the genetic algorithm. Later, with the purpose of validation, we determine the stress–stretch relation, and determine the temperature change in another series of experiments, and draw comparisons with the model predictions. The results show that the material behavior strongly depends on the temperature, strain rate and also the fiber's direction. We determine that the temperature change is more significant at high strain rate and initial temperature levels and that it is necessary to use the developed coupled model.

1. Introduction

Thermal ablation and hyperthermia of tumors consists in the local application of extreme temperatures, which can be either high or low, to induce irreversible injury [1]. This method can be utilized to cure soft tissue diseases [2–4]. The procedure is to apply controlled temperature elevation by targeting the heating field to the cancerous tumor and the enclosing tissue [5].

Most hyperthermic investigations have concentrated on the tumoricidal effects of heat at 42–44 °C because at these temperatures cancerous tissue has been observed to be more sensitive [6,7]. Although elevated temperatures may have therapeutic benefit, host tissue tolerance is a limiting factor due to the irreversible damage to both normal and neoplastic tissues [8] which should be evaluated in the surrounding soft tissues. Beside experimental observations, thermo-mechanical constitutive models can be employed to simulate soft tissues hyperthermia. This simulation requires a thermo-mechanical basis.

To model soft tissues, a wide variety of studies utilize the isotropic [9–11] and anisotropic hyperelastic energy functions [12,13] concerning isothermal applications. To implement the anisotropic simulation of biological tissues, several scholars have set the response as the sum of matrix and fiber energy functions [14,15]. To capture the anisotropic behavior of fiber-reinforced tissues, Gasser–Ogden–Holzapfel (GOH) and Fung-type energy functions are popular [16–18]. In the absence of viscous effects, these models are consistent with experimental results.

For modeling the viscous behavior of soft tissues, it is essential to consider the rate-dependent response of the material. The rate-dependent response can be divided into equilibrium (elastic) and non-equilibrium (viscous) parts. More sophisticated approaches have been developed to simulate visco-hyperelastic isotropic [19,20] and anisotropic [21–24] response of soft tissues. Among different techniques, decoupling the Helmholtz free energy function into an elastic and a viscous component for matrix and fiber is a successful method [25,26].

To involve the effect of temperature in the elastic [27] or viscoelastic [28–32] models, most of biomechanical studies recommend a linear function for properties with the temperature. In other researches, the structure of temperature dependent free energy functions has been introduced and implemented using a thermodynamical view [33,34]. Although considering the thermal influences on properties and energy functions will improve model accuracy, potential damage which may be induced by the excessive temperature should also be considered.

Despite many notable articles on visco-hyperelastic-damage formulation [35–38], based on a literature survey by Li [39] and to the best of our knowledge, the temperature and damage coupled effect in the thermo-visco-hyperelastic modeling of fibrous soft tissues has not been thoroughly addressed yet. Hence, in this paper, rate-dependent damage and thermo-visco-hyperelastic response are coupled. For this purpose, in the first section, based on the thermodynamics in the thermal dilated configuration, we develop the rheological model and the coupled thermo-mechanical equation. The temperature terms are

* Corresponding author.
E-mail address: f_vakili@tabrizu.ac.ir (F. Vakili-Tahami).

https://doi.org/10.1016/j.ijnonlinmec.2019.103260
Received 4 June 2019; Received in revised form 26 August 2019; Accepted 29 August 2019
Available online 2 September 2019

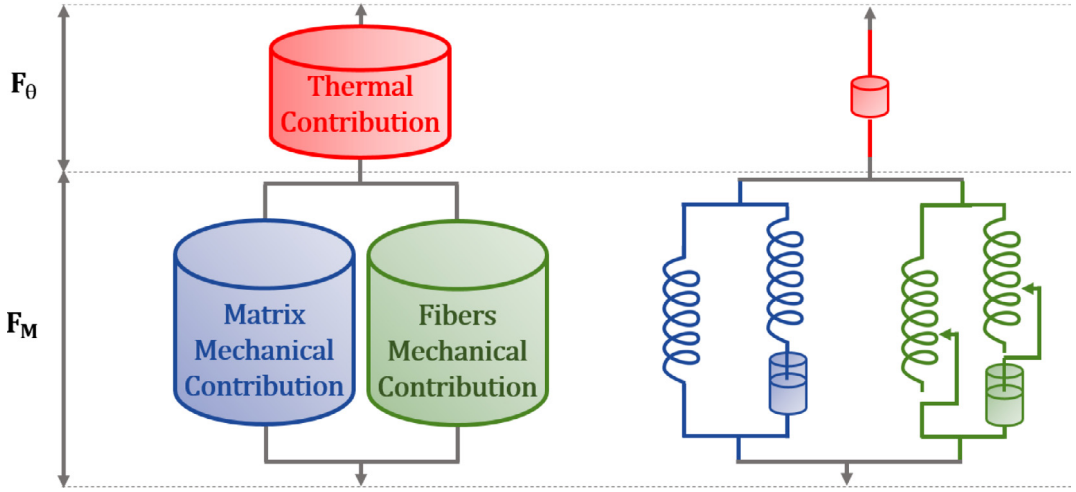

Fig. 1. Rheological model.

merged in the matrix (isotropic) and fiber (anisotropic) energy functions, viscous flow rule, and rate-dependent damage. We perform a set of cyclic experiments at different temperatures and strain rates on bovine round muscle to verify the model and to obtain the material parameters. The Genetic Algorithm (GA) is employed to determine the material parameters. Also, we use another set of experiments to validate the model.

2. Thermal and damage coupled rheological model

The developed constitutive rheological model is composed of thermal and mechanical branches of the matrix and fibers as shown in Fig. 1. This model evaluates the damage by coupling thermal and mechanical effects of fibrous tissues.

2.1. Kinematic decomposition

To describe the kinematics of the model, according to Fig. 2, four steps can be considered, which connect the reference configuration Ω_0 to the current one Ω. Two intermediate steps $\overline{\Omega}_\theta$ and $\overline{\Omega}$ indicate the thermal dilated and the relaxed configurations respectively. The deformation gradient tensor $\mathbf{F}$ as a function of time (t) may be used to map an element from the reference configuration to the current step:

$$\mathbf{F}(\mathbf{X},t) = F_{iA}\mathbf{e}_i \otimes \mathbf{e}_A = \frac{\partial x_i}{\partial X_A}\mathbf{e}_i \otimes \mathbf{e}_A \tag{1}$$

in which x_i and X_A refer to the spatial (current) and material (reference) coordinates of each particle respectively, $\mathbf{e}$ is the unit vector and $\otimes$ is the tensor product. Inspired by other researchers [40–42] and according to Fig. 1, the deformation gradient tensor can be decomposed multiplicatively into a thermal $\mathbf{F}_\theta$ and a mechanical $\mathbf{F}_M$ part:

$$\mathbf{F} = \mathbf{F}_M\mathbf{F}_\theta \tag{2}$$

The mechanical deformation gradient tensor, $\mathbf{F}_M$ will affect the matrix behavior $\mathbf{F}_M^m$ as well as the fibers $\mathbf{F}_M^f$. Since the model has a parallel arrangement (Fig. 1), $\mathbf{F}_M^m$ and $\mathbf{F}_M^f$ will be equal:

$$\mathbf{F}_M = \mathbf{F}_M^m = \mathbf{F}_M^f \tag{3}$$

The matrix and fiber contributions are divided into purely elastic ($\mathbf{F}_\mathcal{E}^i$) and viscoelastic ($\mathbf{F}_V^i$) parts:

$$\mathbf{F}_M^i = \mathbf{F}_\mathcal{E}^i = \mathbf{F}_V^i \quad i = m \text{ and } f \tag{4}$$

where m and f superscripts identify matrix and fiber respectively. The viscoelastic deformation gradient is assumed to be composed as:

$$\mathbf{F}_V^i = \mathbf{F}_V^{i,\mathcal{E}}\mathbf{F}_V^{i,v} \quad i = m \text{ and } f \tag{5}$$

where $\mathbf{F}_V^{i,\mathcal{E}}$ and $\mathbf{F}_V^{i,v}$ are elastic and viscous parts of the viscoelastic deformation gradient tensor. Merging equations (2), (4) and (5) leads to:

$$\mathbf{F}^i = \mathbf{F}_V^{i,\mathcal{E}}\mathbf{F}_V^{i,v}\mathbf{F}_\theta = \mathbf{F}_\mathcal{E}^i\mathbf{F}_\theta \quad i = m \text{ and } f \tag{6}$$

The velocity gradient tensor of a continuum ($\mathbf{l}$) is [43]:

$$\mathbf{l} = \dot{\mathbf{F}}\mathbf{F}^{-1} \tag{7}$$

This tensor can be decomposed to the rate of stretching ($\mathbf{d}$) and the spin tensor ($\boldsymbol{\omega}$):

$$\mathbf{l} = \mathbf{d} + \boldsymbol{\omega} \tag{8}$$

in which $\mathbf{d}$ and $\boldsymbol{\omega}$ are symmetric and skew-symmetric parts of $\mathbf{l}$ respectively:

$$\mathbf{d} = \frac{\mathbf{l} + \mathbf{l}^T}{2} \tag{9}$$

$$\boldsymbol{\omega} = \frac{\mathbf{l} - \mathbf{l}^T}{2} \tag{10}$$

where superscript T denotes transpose. Considering Eqs. (6) and (7), thermo-viscous velocity tensor ($\mathbf{l}_{\theta V}$) can be written as:

$$\begin{aligned}\mathbf{l}_{\theta V} &= \left(\dot{\mathbf{F}}_V^{i,\mathcal{E}}\mathbf{F}_V^{i,v}\mathbf{F}_\theta + \mathbf{F}_V^{i,\mathcal{E}}\dot{\mathbf{F}}_V^{i,v}\mathbf{F}_\theta + \mathbf{F}_V^{i,\mathcal{E}}\mathbf{F}_V^{i,v}\dot{\mathbf{F}}_\theta\right)\mathbf{F}_\theta^{-1}\mathbf{F}_V^{-i,v}\mathbf{F}_V^{-i,\mathcal{E}} \\ &= \dot{\mathbf{F}}_V^{i,\mathcal{E}}\mathbf{F}_V^{-i,\mathcal{E}} + \mathbf{F}_V^{i,\mathcal{E}}\dot{\mathbf{F}}_V^{i,v}\mathbf{F}_V^{-i,v}\mathbf{F}_V^{-i,\mathcal{E}} + \mathbf{F}_V^{i,\mathcal{E}}\mathbf{F}_V^{i,v}\dot{\mathbf{F}}_\theta\mathbf{F}_\theta^{-1}\mathbf{F}_V^{-i,v}\mathbf{F}_V^{-i,\mathcal{E}} \\ &= \mathbf{l}_V^{i,\mathcal{E}} + \mathbf{F}_V^{i,\mathcal{E}}\bar{\mathbf{l}}_V^{i,v}\mathbf{F}_V^{-i,\mathcal{E}} + \mathbf{F}_V^{i,\mathcal{E}}\mathbf{F}_V^{i,v}\bar{\mathbf{l}}_\theta\mathbf{F}_V^{-i,v}\mathbf{F}_V^{-i,\mathcal{E}} \quad i = m \text{ and } f\end{aligned} \tag{11}$$

in which $\mathbf{l}_V^{i,\mathcal{E}} = \dot{\mathbf{F}}_V^{i,\mathcal{E}}\mathbf{F}_V^{-i,\mathcal{E}}$, $\bar{\mathbf{l}}_V^{i,v} = \dot{\mathbf{F}}_V^{i,v}\mathbf{F}_V^{-i,v}$ are elastic and viscous parts ($\mathbf{l}_V = \mathbf{l}_V^{i,\mathcal{E}} + \mathbf{F}_V^{i,\mathcal{E}}\bar{\mathbf{l}}_V^{i,v}\mathbf{F}_V^{-i,\mathcal{E}}$). In this equation $\bar{\mathbf{l}}_\theta = \dot{\mathbf{F}}_\theta\mathbf{F}_\theta^{-1}$ is the thermal velocity tensor. In a similar way, the thermo-elastic velocity tensor ($\mathbf{l}_{\theta\mathcal{E}}$) is as follows:

$$\begin{aligned}\mathbf{l}_{\theta\mathcal{E}} &= \left(\dot{\mathbf{F}}_\mathcal{E}^i\mathbf{F}_\theta + \mathbf{F}_\mathcal{E}^i\dot{\mathbf{F}}_\theta\right)\mathbf{F}_\theta^{-1}\mathbf{F}_\mathcal{E}^{-i} \\ &= \dot{\mathbf{F}}_\mathcal{E}^i\mathbf{F}_\mathcal{E}^{-i} + \mathbf{F}_\mathcal{E}^i\dot{\mathbf{F}}_\theta\mathbf{F}_\theta^{-1}\mathbf{F}_\mathcal{E}^{-i} \\ &= \mathbf{l}_\mathcal{E}^i + \mathbf{F}_\mathcal{E}^i\bar{\mathbf{l}}_\theta\mathbf{F}_\mathcal{E}^{-i} \quad i = m \text{ and } f\end{aligned} \tag{12}$$

where $\mathbf{l}_\mathcal{E}^i = \dot{\mathbf{F}}_\mathcal{E}^i\mathbf{F}_\mathcal{E}^{-i}$ is the pure elastic velocity tensor.

2.2. Thermodynamics framework

In this subsection, by using the first and second thermodynamic principles, we study the consistency of the model. Produced entropy (H) by a continuum is equal to [44]:

$$H(t) = \int_\Omega \eta(x,t)\,dV \tag{13}$$

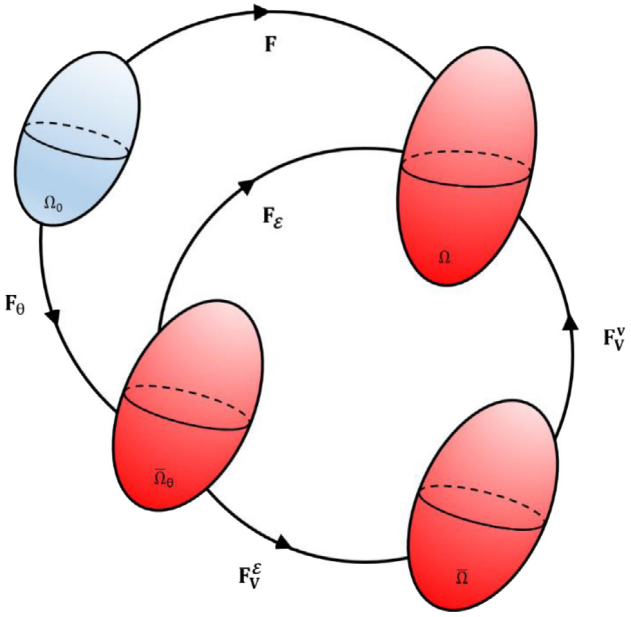

Fig. 2. Deformation kinematic decomposition.

in which η is the entropy per unit current volume. Temporal change of H has two contributions, the reversible (due to the external heat sources) and the irreversible (due to the dissipation) parts. The second law of thermodynamics states that the irreversible part is never negative, which leads to the well-known Clausius–Duhemprinciple [45,46] inequality in the current configuration (Ω).

Considering that V, $\overline{\mathrm{V}}_\theta$ and V_0 are current, thermal dilated and reference volumes respectively, one can write $\mathrm{dV} = \mathrm{J}_\mathrm{M}\mathrm{d}\overline{\mathrm{V}}_\theta = \mathrm{J}\mathrm{dV}_0$ where $\mathrm{J} = \mathrm{J}_\mathrm{M}\mathrm{J}_\theta = \det(\mathbf{F})$, $\mathrm{J}_\mathrm{M} = \det(\mathbf{F}_\mathrm{M})$ and $\mathrm{J}_\theta = \det(\mathbf{F}_\theta)$ are Jacobian determinants. Therefore temporal change of H can be written as:

$$\frac{\mathrm{D}}{\mathrm{Dt}}\int_\Omega \eta \mathrm{dV} = \frac{\mathrm{D}}{\mathrm{Dt}}\int_{\overline{\Omega}_\theta} \eta \mathrm{d}\overline{\mathrm{V}}_\theta = \int_{\overline{\Omega}_\theta}\left(\dot{\overline{\eta}} + \overline{\eta}\mathrm{J}_\theta^{-1}\frac{\partial \mathrm{J}_\theta}{\partial \mathrm{t}}\right)\mathrm{d}\overline{\mathrm{V}}_\theta \tag{14}$$

Introducing isotropic thermal expansion coefficient (α_θ) [47]:

$$\mathbf{F}_\theta = \mathrm{e}^{\alpha_\theta\theta}\mathbf{I} \cong \left(1+\alpha_\theta\theta\right)\mathbf{I} \tag{15}$$

where $\mathbf{I}$ and θ are unit matrix and temperature. According to Eq. (8) one can write:

$$\bar{\mathbf{l}}_\theta = \dot{\mathbf{F}}_\theta\mathbf{F}_\theta^{-1} = \mathrm{f}_\theta\dot{\theta}\mathbf{I} \tag{16}$$

in which $\mathrm{f}_\theta = \frac{\frac{\partial\alpha_\theta}{\partial\theta}\theta+\alpha_\theta}{1+\alpha_\theta\theta}$ is a temperature dependent function of α_θ. Considering (9), (10) and (16) indicates that $\overline{\boldsymbol{\omega}}_\theta = \mathbf{0}$ and $\bar{\mathbf{l}}_\theta = \bar{\mathbf{d}}_\theta$ in which $\bar{\mathbf{d}}_\theta$ is thermal rate of stretching. Also, $\mathrm{J}_\theta^{-1}\frac{\partial \mathrm{J}_\theta}{\partial \mathrm{t}} = \mathrm{tr}\left(\bar{\mathbf{d}}_\theta\right) = 3\mathrm{f}_\theta\dot{\theta}$.

Therefore the Clausius-Duhem inequality in the $\overline{\Omega}_\theta$ configuration can be written as:

$$\dot{\overline{\eta}} + \overline{\eta}\mathrm{tr}\left(\bar{\mathbf{d}}_\theta\right) + \frac{1}{\theta}\overline{\nabla}.\overline{\mathbf{Q}} - \frac{1}{\theta^2}\overline{\mathbf{Q}}.\overline{\nabla}\theta - \frac{\overline{\mathrm{R}}}{\theta} \geq 0 \tag{17}$$

in which $\overline{\mathbf{Q}}$ and $\overline{\mathrm{R}}$ are the Piola–Kirchhoff heat flux per unit surface area and the heat sources per unit volume in $\overline{\Omega}_\theta$ respectively.

Implementing the first law of thermodynamics, the energy balance in $\overline{\Omega}_\theta$, can be written as follows:

$$\int_{\overline{\Omega}_\theta}\left(\dot{\bar{e}} + \bar{e}\mathrm{tr}\left(\bar{\mathbf{d}}_\theta\right)\right)\mathrm{d}\overline{\mathrm{V}}_\theta = \int_{\overline{\Omega}_\theta}\left[\boldsymbol{\sigma}:\mathbf{l} - \mathrm{div}\left(\mathbf{q}\right) + \mathrm{r}\right]\mathrm{J}_\mathrm{M}\mathrm{d}\overline{\mathrm{V}}_\theta \tag{18}$$

where $\boldsymbol{\sigma}$, $\mathbf{q}$, r and $\bar{e}$ are the Cauchy stress, heat source, heat flux, and specific internal energy per unit volume respectively. Using the Helmholtz free energy per unit volume ($\overline{\Psi}$), the specific internal energy ($\bar{e}$) is divided as [44]:

$$\bar{e} = \overline{\Psi} + \theta\overline{\eta} \tag{19}$$

Based on the rule of mixture, we can decompose stress into matrix and fiber parts as [48]:

$$\boldsymbol{\sigma} = \sum_{\mathrm{i=m\ and\ f}} \boldsymbol{\sigma}^\mathrm{i} \tag{20}$$

2.3. Formulation of the model

In this paper, we model fibrous soft tissue damage coupled with the thermal and mechanical effects based on visco-hyperelasticity. The proposed model deals with the time and temperature dependent behavior of tissue (Fig. 1) including an equilibrium (elastic) and a non-equilibrium (viscoelastic) responses. For this purpose, we employ the first law of thermodynamics and the Clausius-Duhem inequality.

The stress power ($\boldsymbol{\sigma}:\mathbf{l}$) in the left hand side of Eq. (18) can be calculated utilizing equations (11), (12) and (20) as:

$$\begin{aligned}\boldsymbol{\sigma}:\mathbf{l} &= \sum_{\mathrm{i=m\ and\ f}} \boldsymbol{\sigma}_\mathrm{V}^\mathrm{i}:\mathbf{l}_{\theta\mathrm{V}} + \boldsymbol{\sigma}_\mathcal{E}^\mathrm{i}:\mathbf{l}_{\theta\mathcal{E}} \\ &= \sum_{\mathrm{i=m\ and\ f}} \Big(\boldsymbol{\sigma}_\mathrm{V}^\mathrm{i}:\mathbf{l}_\mathrm{V}^{\mathrm{i},\mathcal{E}} + \boldsymbol{\sigma}_\mathrm{V}^\mathrm{i}:\mathbf{F}_\mathrm{V}^{\mathrm{i},\mathcal{E}}\bar{\mathbf{l}}_\mathrm{V}^{\mathrm{i,v}}\mathbf{F}_\mathrm{V}^{-\mathrm{i},\mathcal{E}} \\ &\quad + \boldsymbol{\sigma}_\mathrm{V}^\mathrm{i}:\mathbf{F}_\mathrm{V}^{\mathrm{i},\mathcal{E}}\mathbf{F}_\mathrm{V}^{\mathrm{i,v}}\bar{\mathbf{l}}_\theta\mathbf{F}_\mathrm{V}^{-\mathrm{i,v}}\mathbf{F}_\mathrm{V}^{-\mathrm{i},\mathcal{E}} + \boldsymbol{\sigma}_\mathcal{E}^\mathrm{i}:\mathbf{l}_\mathcal{E}^\mathrm{i} \\ &\quad + \boldsymbol{\sigma}_\mathcal{E}^\mathrm{i}:\mathbf{F}_\mathcal{E}^\mathrm{i}\bar{\mathbf{l}}_\theta\mathbf{F}_\mathcal{E}^{-\mathrm{i}}\Big)\end{aligned} \tag{21}$$

where $\boldsymbol{\sigma}_\mathrm{V}^\mathrm{i}$ and $\boldsymbol{\sigma}_\mathcal{E}^\mathrm{i}$ are viscous and elastic Cauchy stresses.

Knowing that the inner product of symmetric and skew-symmetric second order tensor is zero and considering that $\boldsymbol{\sigma}$ is a second order symmetric tensor, according to Eq. (8) we can write [43]:

$$\boldsymbol{\sigma}:\mathbf{l} = \boldsymbol{\sigma}:\mathbf{d} + \boldsymbol{\sigma}:\mathbf{w} = \boldsymbol{\sigma}:\mathbf{d} \tag{22}$$

Adopting equation (22), the second Piola–Kirchhoff stress $\mathbf{S} = \mathrm{J}\mathbf{F}^{-1}\boldsymbol{\sigma}\mathbf{F}^{-\mathrm{T}}$ and the Mandel stress $\mathbf{M} = \mathbf{F}^\mathrm{T}\mathbf{F}\mathbf{S}$, the stress power per unit volume in $\overline{\Omega}_\theta$, is obtained as follows:

$$\begin{aligned}\boldsymbol{\sigma}:\mathbf{d} = \sum_{\mathrm{i=m\ and\ f}} \mathrm{J}_\mathrm{M}^{-1}\Big(&\bar{\mathbf{S}}_\mathrm{V}^\mathrm{i}:\mathbf{F}_\mathrm{M}^\mathrm{T}\mathbf{d}_\mathrm{V}^{\mathrm{i},\mathcal{E}}\mathbf{F}_\mathrm{M} + \overline{\mathbf{M}}_\mathrm{V}^\mathrm{i}:\bar{\mathbf{d}}_\mathrm{V}^{\mathrm{i,v}} + \overline{\mathbf{M}}_\mathrm{V}^\mathrm{i}:\bar{\mathbf{d}}_\theta \\ &+\bar{\mathbf{S}}_\mathcal{E}^\mathrm{i}:\mathbf{F}_\mathrm{M}^\mathrm{T}\mathbf{d}_\mathcal{E}^\mathrm{i}\mathbf{F}_\mathrm{M} + \overline{\mathbf{M}}_\mathcal{E}^\mathrm{i}:\bar{\mathbf{d}}_\theta\Big)\end{aligned} \tag{23}$$

where $\overline{\mathbf{M}}_\mathrm{V}^\mathrm{i} = \mathbf{F}_\mathrm{M}^\mathrm{T}\mathbf{F}_\mathrm{M}\bar{\mathbf{S}}_\mathrm{V}^\mathrm{i} = \mathbf{F}_\mathrm{V}^{\mathrm{i,v}\mathrm{T}}\mathbf{C}_\mathrm{V}^{\mathrm{i},\mathcal{E}}\mathbf{F}_\mathrm{V}^{\mathrm{i,v}}\bar{\mathbf{S}}_\mathrm{V}^\mathrm{i}$ and $\overline{\mathbf{M}}_\mathcal{E}^\mathrm{i} = \mathbf{F}_\mathcal{E}^{\mathrm{iT}}\mathbf{F}_\mathcal{E}^\mathrm{i}\bar{\mathbf{S}}_\mathcal{E}^\mathrm{i} = \mathbf{C}_\mathcal{E}^\mathrm{i}\bar{\mathbf{S}}_\mathcal{E}^\mathrm{i}$ in which $\mathbf{C}_\mathrm{V}^{\mathrm{i},\mathcal{E}} = \mathbf{F}_\mathrm{V}^{\mathrm{i},\mathcal{E}\mathrm{T}}\mathbf{F}_\mathrm{V}^{\mathrm{i},\mathcal{E}}$ and $\mathbf{C}_\mathcal{E}^\mathrm{i} = \mathbf{F}_\mathcal{E}^{\mathrm{i},\mathrm{T}}\mathbf{F}_\mathcal{E}^\mathrm{i}$ are elastic right-Cauchy–Green deformation tensors respectively. $\mathbf{d}_\mathrm{V}^{\mathrm{i},\mathcal{E}}$, $\mathbf{d}_\mathcal{E}^\mathrm{i}$ and $\bar{\mathbf{d}}_\mathrm{V}^{\mathrm{i,v}}$ are the elastic and viscous rate of stretching.

By using Eqs. (17), (18), (19) and (23), the Clausius-Duhem inequality will be read as:

$$\begin{aligned}&\sum_{\mathrm{i=m\ and\ f}}\Big(\bar{\mathbf{S}}_\mathrm{V}^\mathrm{i}:\mathbf{F}_\mathrm{M}^\mathrm{T}\mathbf{d}_\mathrm{V}^{\mathrm{i},\mathcal{E}}\mathbf{F}_\mathrm{M} + \overline{\mathbf{M}}_\mathrm{V}^\mathrm{i}:\bar{\mathbf{d}}_\mathrm{V}^{\mathrm{i,v}} + \overline{\mathbf{M}}_\mathrm{V}^\mathrm{i}:\bar{\mathbf{d}}_\theta + \bar{\mathbf{S}}_\mathcal{E}^\mathrm{i}:\mathbf{F}_\mathrm{M}^\mathrm{T}\mathbf{d}_\mathcal{E}^\mathrm{i}\mathbf{F}_\mathrm{M} \\ &+\overline{\mathbf{M}}_\mathcal{E}^\mathrm{i}:\bar{\mathbf{d}}_\theta\Big) - \dot{\overline{\Psi}} - \overline{\Psi}\mathrm{tr}\left(\bar{\mathbf{d}}_\theta\right) \\ &- \dot{\theta}\overline{\eta} - \frac{1}{\theta}\overline{\mathbf{Q}}.\overline{\nabla}\theta \geq 0\end{aligned} \tag{24}$$

The Helmholtz free energy function is assumed to be a function of the elastic right-Cauchy–Green deformation tensors of matrix and fiber ($\mathbf{C}_\mathcal{E}^\mathrm{m}, \mathbf{C}_\mathrm{V}^{\mathrm{m},\mathcal{E}}, \mathbf{C}_\mathcal{E}^\mathrm{f}$ and $\mathbf{C}_\mathrm{V}^{\mathrm{f},\mathcal{E}}$), temperature ($\theta$), structure tensor ($\mathbf{A}_0$) and damage of matrix ($\xi^\mathrm{m}$) and fiber ($\xi^\mathrm{f}$):

$$\overline{\Psi} = \overline{\Psi}\left(\mathbf{C}_\mathrm{V}^{\mathrm{m},\mathcal{E}}, \mathbf{C}_\mathcal{E}^\mathrm{m}, \mathbf{C}_\mathrm{V}^{\mathrm{f},\mathcal{E}}, \mathbf{C}_\mathcal{E}^\mathrm{f}, \theta, \mathbf{A}_0, \xi^\mathrm{m}, \xi^\mathrm{f}\right) \tag{25}$$

where

$$\mathbf{A}_0 = \boldsymbol{a}_0 \otimes \boldsymbol{a}_0 \tag{26}$$

and $\boldsymbol{a}_0$ is the fiber direction unit vector. Thus, $\dot{\overline{\Psi}}$ is determined as:

$$\begin{aligned}\dot{\overline{\Psi}} = &\frac{\partial\overline{\Psi}}{\partial\mathbf{C}_\mathrm{V}^{\mathrm{m},\mathcal{E}}}:\dot{\mathbf{C}}_\mathrm{V}^{\mathrm{m},\mathcal{E}} + \frac{\partial\overline{\Psi}}{\partial\mathbf{C}_\mathcal{E}^\mathrm{m}}:\dot{\mathbf{C}}_\mathcal{E}^\mathrm{m} + \frac{\partial\overline{\Psi}}{\partial\mathbf{C}_\mathrm{V}^{\mathrm{f},\mathcal{E}}}:\dot{\mathbf{C}}_\mathrm{V}^{\mathrm{f},\mathcal{E}} + \frac{\partial\overline{\Psi}}{\partial\mathbf{C}_\mathcal{E}^\mathrm{f}}:\dot{\mathbf{C}}_\mathcal{E}^\mathrm{f} + \frac{\partial\overline{\Psi}}{\partial\theta}\dot{\theta} \\ &+ \frac{\partial\overline{\Psi}}{\partial\xi^\mathrm{m}}\dot{\xi}^\mathrm{m} + \frac{\partial\overline{\Psi}}{\partial\xi^\mathrm{f}}\dot{\xi}^\mathrm{f}\end{aligned} \tag{27}$$

Substituting Eq. (27) in (24) and considering that:

$$\frac{\partial\overline{\Psi}}{\partial\mathbf{C}_{\mathrm{V}}^{\mathrm{i},\mathcal{E}}}:\dot{\mathbf{C}}_{\mathrm{V}}^{\mathrm{i},\mathcal{E}}=\frac{\partial\overline{\Psi}}{\partial\mathbf{C}_{\mathrm{V}}^{\mathrm{i},\mathcal{E}}}:\left(\dot{\mathbf{F}}_{\mathrm{V}}^{\mathrm{i},\mathcal{E},\mathrm{T}}\mathbf{F}_{\mathrm{V}}^{\mathrm{i},\mathcal{E}}+\mathbf{F}_{\mathrm{V}}^{\mathrm{i},\mathcal{E},\mathrm{T}}\dot{\mathbf{F}}_{\mathrm{V}}^{\mathrm{i},\mathcal{E}}\right)=2\frac{\partial\overline{\Psi}}{\partial\mathbf{C}_{\mathrm{V}}^{\mathrm{i},\mathcal{E}}}:\mathbf{F}_{\mathrm{V}}^{\mathrm{i},\mathcal{E},\mathrm{T}}\mathbf{d}_{\mathrm{V}}^{\mathrm{i},\mathcal{E}}\mathbf{F}_{\mathrm{V}}^{\mathrm{i},\mathcal{E}} \tag{28}$$

$$\frac{\partial\overline{\Psi}}{\partial\mathbf{C}_{\mathcal{E}}^{\mathrm{i}}}:\dot{\mathbf{C}}_{\mathcal{E}}^{\mathrm{i}}=\frac{\partial\overline{\Psi}}{\partial\mathbf{C}_{\mathcal{E}}^{\mathrm{i}}}:\left(\dot{\mathbf{F}}_{\mathcal{E}}^{\mathrm{i},\mathrm{T}}\mathbf{F}_{\mathcal{E}}^{\mathrm{i}}+\mathbf{F}_{\mathcal{E}}^{\mathrm{i},\mathrm{T}}\dot{\mathbf{F}}_{\mathcal{E}}^{\mathrm{i}}\right)=2\frac{\partial\overline{\Psi}}{\partial\mathbf{C}_{\mathcal{E}}^{\mathrm{i}}}:\mathbf{F}_{\mathcal{E}}^{\mathrm{i},\mathrm{T}}\mathbf{d}_{\mathcal{E}}^{\mathrm{i}}\mathbf{F}_{\mathcal{E}}^{\mathrm{i}} \tag{29}$$

we can write:

$$\begin{aligned}&\left(\overline{\mathbf{S}}_{\mathcal{E}}^{\mathrm{m}}-2\frac{\partial\overline{\Psi}}{\partial\mathbf{C}_{\mathcal{E}}^{\mathrm{m}}}\right)\\&:\mathbf{F}_{\mathcal{E}}^{\mathrm{m},\mathrm{T}}\mathbf{d}_{\mathcal{E}}^{\mathrm{m}}\mathbf{F}_{\mathcal{E}}^{\mathrm{m}}+\left(\mathbf{F}_{\mathrm{V}}^{\mathrm{m},\mathrm{v}}\overline{\mathbf{S}}_{\mathrm{V}}^{\mathrm{m}}\mathbf{F}_{\mathrm{V}}^{\mathrm{m},\mathrm{v},\mathrm{T}}-2\frac{\partial\overline{\Psi}}{\partial\mathbf{C}_{\mathrm{V}}^{\mathrm{m},\mathcal{E}}}\right):\mathbf{F}_{\mathrm{V}}^{\mathrm{m},\mathcal{E}\mathrm{T}}\mathbf{d}_{\mathrm{V}}^{\mathrm{m},\mathcal{E}}\mathbf{F}_{\mathrm{V}}^{\mathrm{m},\mathcal{E}}\\&+\left(\overline{\mathbf{S}}_{\mathcal{E}}^{\mathrm{f}}-2\frac{\partial\overline{\Psi}}{\partial\mathbf{C}_{\mathcal{E}}^{\mathrm{f}}}\right):\mathbf{F}_{\mathcal{E}}^{\mathrm{f},\mathrm{T}}\mathbf{d}_{\mathcal{E}}^{\mathrm{f}}\mathbf{F}_{\mathcal{E}}^{\mathrm{f}}+\left(\mathbf{F}_{\mathrm{V}}^{\mathrm{f},\mathrm{v}}\overline{\mathbf{S}}_{\mathrm{V}}^{\mathrm{f}}\mathbf{F}_{\mathrm{V}}^{\mathrm{f},\mathrm{v}\mathrm{T}}-2\frac{\partial\overline{\Psi}}{\partial\mathbf{C}_{\mathrm{V}}^{\mathrm{f},\mathcal{E}}}\right):\\&\mathbf{F}_{\mathrm{V}}^{\mathrm{f},\mathcal{E}\mathrm{T}}\mathbf{d}_{\mathrm{V}}^{\mathrm{f},\mathcal{E}}\mathbf{F}_{\mathrm{V}}^{\mathrm{f},\mathcal{E}}\\&+\overline{\mathbf{M}}_{\mathrm{V}}^{\mathrm{m}}:\dot{\mathbf{d}}_{\mathrm{V}}^{\mathrm{m},\mathrm{v}}+\overline{\mathbf{M}}_{\mathrm{V}}^{\mathrm{f}}:\dot{\mathbf{d}}_{\mathrm{V}}^{\mathrm{f},\mathrm{v}}+\frac{\partial\overline{\Psi}}{\partial\xi^{\mathrm{m}}}\dot{\xi}^{\mathrm{m}}+\frac{\partial\overline{\Psi}}{\partial\xi^{\mathrm{f}}}\dot{\xi}^{\mathrm{f}}-\frac{1}{\theta}\overline{\mathbf{Q}}.\overline{\nabla}\theta\\&+\left[\alpha_{\theta}\left(\overline{\mathbf{M}}_{\mathrm{V}}^{\mathrm{m}}+\overline{\mathbf{M}}_{\mathcal{E}}^{\mathrm{m}}+\overline{\mathbf{M}}_{\mathrm{V}}^{\mathrm{f}}+\overline{\mathbf{M}}_{\mathcal{E}}^{\mathrm{f}}\right):\mathbf{I}-\frac{\partial\overline{\Psi}}{\partial\theta}-3\alpha_{\theta}\overline{\Psi}-\overline{\eta}\right]\dot{\theta}\geq 0\end{aligned} \tag{30}$$

This inequality must hold for any arbitrary values; therefore, by using the Coleman and Noll [49] common procedure, we can write:

$$\overline{\mathbf{S}}_{\mathcal{E}}^{\mathrm{i}}=2\frac{\partial\overline{\Psi}}{\partial\mathbf{C}_{\mathcal{E}}^{\mathrm{i}}}\qquad\mathrm{i}=\mathrm{m}\text{ and }\mathrm{f} \tag{31}$$

$$\overline{\mathbf{S}}_{\mathrm{V}}^{\mathrm{i}}=2\mathbf{F}_{\mathrm{V}}^{-\mathrm{i},\mathrm{v}}\frac{\partial\overline{\Psi}}{\partial\mathbf{C}_{\mathrm{V}}^{\mathrm{i},\mathcal{E}}}\mathbf{F}_{\mathrm{V}}^{-\mathrm{i},\mathrm{v}\mathrm{T}}\qquad\mathrm{i}=\mathrm{m}\text{ and }\mathrm{f} \tag{32}$$

$$\overline{\eta}=\alpha_{\theta}\sum_{\mathrm{i=m\ and\ f}}\left(\overline{\mathbf{M}}_{\mathcal{E}}^{\mathrm{i}}+\overline{\mathbf{M}}_{\mathrm{V}}^{\mathrm{i}}\right):\mathbf{I}-\frac{\partial\overline{\Psi}}{\partial\theta}-3\alpha_{\theta}\overline{\Psi} \tag{33}$$

Hence the inequality (30) is reduced to (34) to calculate the dissipation ($\overline{D}$):

$$\overline{D}=\sum_{\mathrm{i=m\ and\ f}}\left(\overline{\mathbf{M}}_{\mathrm{V}}^{\mathrm{i}}:\dot{\overline{\mathbf{d}}}_{\mathrm{V}}^{\mathrm{i},\mathrm{v}}\right)-\frac{\partial\overline{\Psi}}{\partial\xi^{\mathrm{m}}}\dot{\xi}^{\mathrm{m}}-\frac{\partial\overline{\Psi}}{\partial\xi^{\mathrm{f}}}\dot{\xi}^{\mathrm{f}}-\frac{1}{\theta}\overline{\mathbf{Q}}.\overline{\nabla}\theta\geq 0 \tag{34}$$

This inequality is divided into two parts, the intrinsic $\overline{D}_I$ and thermal dissipations $\overline{D}_\theta$:

$$\overline{D}_{\mathrm{I}}=\sum_{\mathrm{i=m\ and\ f}}\left(\overline{\mathbf{M}}_{\mathrm{V}}^{\mathrm{i}}:\dot{\overline{\mathbf{d}}}_{\mathrm{V}}^{\mathrm{i},\mathrm{v}}\right)-\frac{\partial\overline{\Psi}}{\partial\xi^{\mathrm{m}}}\dot{\xi}^{\mathrm{m}}-\frac{\partial\overline{\Psi}}{\partial\xi^{\mathrm{f}}}\dot{\xi}^{\mathrm{f}}\geq 0 \tag{35}$$

$$\overline{D}_{\theta}=\frac{1}{\theta}\overline{\mathbf{Q}}.\overline{\nabla}\theta\geq 0 \tag{36}$$

The first term in Eq. (35) is due to the viscoelastic response and the other ones are damage dissipation terms. Also, $\overline{D}_\theta$ is associated with the irreversible energy flow. Combining equations (18), (19) and (23) results in energy balance as follows:

$$\begin{aligned}&\sum_{\mathrm{i=m\ and\ f}}\left(\overline{\mathbf{S}}_{\mathrm{V}}^{\mathrm{i}}:\mathbf{F}_{\mathrm{M}}^{\mathrm{T}}\mathbf{d}_{\mathrm{V}}^{\mathrm{i},\mathcal{E}}\mathbf{F}_{\mathrm{M}}+\overline{\mathbf{M}}_{\mathrm{V}}^{\mathrm{i}}:\dot{\overline{\mathbf{d}}}_{\mathrm{V}}^{\mathrm{i},\mathrm{v}}+\overline{\mathbf{M}}_{\mathrm{V}}^{\mathrm{i}}:\dot{\overline{\mathbf{d}}}_{\theta}\right.\\&\left.+\overline{\mathbf{S}}_{\mathcal{E}}^{\mathrm{i}}:\mathbf{F}_{\mathrm{M}}^{\mathrm{T}}\mathbf{d}_{\mathcal{E}}^{\mathrm{i}}\mathbf{F}_{\mathrm{M}}+\overline{\mathbf{M}}_{\mathcal{E}}^{\mathrm{i}}:\dot{\overline{\mathbf{d}}}_{\theta}\right)\\&=\theta\dot{\overline{\eta}}+3\alpha_{\theta}\dot{\theta}\theta\overline{\eta}+\dot{\theta}\overline{\eta}+3\alpha_{\theta}\theta\dot{\overline{\Psi}}+\dot{\overline{\Psi}}-\overline{\mathrm{R}}+\overline{\nabla}.\overline{\mathbf{Q}}\end{aligned} \tag{37}$$

With respect to Eq. (33) and given that $\eta=\eta\left(\mathbf{C}_{\mathrm{V}}^{\mathrm{i},\mathcal{E}},\mathbf{C}_{\mathcal{E}}^{\mathrm{i}},\theta,\xi^{\mathrm{m}},\xi^{\mathrm{f}}\right)$:

$$\begin{aligned}\dot{\overline{\eta}}&=\frac{\partial\overline{\eta}}{\partial\mathbf{C}_{\mathrm{V}}^{\mathrm{m},\mathcal{E}}}:\dot{\mathbf{C}}_{\mathrm{V}}^{\mathrm{m},\mathcal{E}}+\frac{\partial\overline{\eta}}{\partial\mathbf{C}_{\mathcal{E}}^{\mathrm{m}}}:\dot{\mathbf{C}}_{\mathcal{E}}^{\mathrm{m}}+\frac{\partial\overline{\eta}}{\partial\mathbf{C}_{\mathrm{V}}^{\mathrm{f},\mathcal{E}}}:\dot{\mathbf{C}}_{\mathrm{V}}^{\mathrm{f},\mathcal{E}}+\frac{\partial\overline{\eta}}{\partial\mathbf{C}_{\mathcal{E}}^{\mathrm{f}}}\\&:\dot{\mathbf{C}}_{\mathcal{E}}^{\mathrm{f}}+\frac{\partial\overline{\eta}}{\partial\theta}\dot{\theta}+\frac{\partial\overline{\eta}}{\partial\xi^{\mathrm{m}}}\dot{\xi}^{\mathrm{m}}+\frac{\partial\overline{\eta}}{\partial\xi^{\mathrm{f}}}\dot{\xi}^{\mathrm{f}}\\&=\sum_{\mathrm{i=m\ and\ f}}\left\{\left[\alpha_{\theta}\frac{\partial\left(\mathbf{F}_{\mathrm{V}}^{\mathrm{i},\mathrm{v}\mathrm{T}}\mathbf{C}_{\mathrm{V}}^{\mathrm{i},\mathcal{E}}\mathbf{F}_{\mathrm{V}}^{\mathrm{i},\mathrm{v}}\overline{\mathbf{S}}_{\mathrm{V}}^{\mathrm{i}}:\mathbf{I}\right)}{\partial\mathbf{C}_{\mathrm{V}}^{\mathrm{i},\mathcal{E}}}-3\alpha_{\theta}\frac{\partial\overline{\Psi}}{\partial\mathbf{C}_{\mathrm{V}}^{\mathrm{i},\mathcal{E}}}-\frac{\partial^{2}\overline{\Psi}}{\partial\theta\partial\mathbf{C}_{\mathrm{V}}^{\mathrm{i},\mathcal{E}}}\right]:\dot{\mathbf{C}}_{\mathrm{V}}^{\mathrm{i},\mathcal{E}}\right.\\&\left.+\left[\alpha_{\theta}\frac{\partial\left(\mathbf{C}_{\mathcal{E}}^{\mathrm{i}}\overline{\mathbf{S}}_{\mathcal{E}}^{\mathrm{i}}:\mathbf{I}\right)}{\partial\mathbf{C}_{\mathcal{E}}^{\mathrm{i}}}-3\alpha_{\theta}\frac{\partial\overline{\Psi}}{\partial\mathbf{C}_{\mathcal{E}}^{\mathrm{i}}}-\frac{\partial^{2}\overline{\Psi}}{\partial\theta\partial\mathbf{C}_{\mathcal{E}}^{\mathrm{i}}}\right]:\dot{\mathbf{C}}_{\mathcal{E}}^{\mathrm{i}}\right\}+\frac{\partial\overline{\eta}}{\partial\theta}\dot{\theta}\\&+\frac{\partial\overline{\eta}}{\partial\xi^{\mathrm{m}}}\dot{\xi}^{\mathrm{m}}+\frac{\partial\overline{\eta}}{\partial\xi^{\mathrm{f}}}\dot{\xi}^{\mathrm{f}}\end{aligned} \tag{38}$$

Also combining equations (27), (28), (29), (33), (35) and (38), the thermo-visco-hyperelastic-damage (TVHD) coupling heat equation is:

$$\left(\dot{\overline{\eta}}+3\alpha_{\theta}\dot{\theta}\overline{\eta}\right)\theta=\overline{\mathcal{D}}_{\mathrm{I}}-\overline{\nabla}.\overline{\mathbf{Q}}+\overline{\mathrm{R}} \tag{39}$$

where $\overline{\mathbf{Q}}$ can be defined using the Duhamel's law of heat conduction:

$$\overline{\mathbf{Q}}=-\mathbf{F}_{\mathrm{M}}^{-1}\kappa_{0}\mathbf{F}_{\mathrm{M}}^{-\mathrm{T}}\mathrm{Grad}\theta \tag{40}$$

in which κ_0 is the conductivity coefficient. To solve the partial differential equation (39), the thermal boundary conditions can be expressed as:

$$-\kappa_{0}\frac{\partial\theta_{\mathrm{b}}}{\partial\mathrm{n}}=\mathrm{h}\left(\theta_{\mathrm{b}}-\theta_{\infty}\right) \tag{41}$$

where θ_b, n, h are the temperature level, normal unit vector and heat transfer coefficient on the boundary respectively and θ_∞ is the ambient temperature.

2.4. Energy functions and flow rules

In most researches, hyperelasticity and visco-hyperelasticity are based on the existence of a free energy function [50–55].

In this study, the free energy function (25), is decoupled into the mechanical ($\overline{\Psi}_{\mathrm{M}}$) and thermal ($\overline{\Psi}_{\theta}$) contributions as:

$$\overline{\Psi}=\overline{\Psi}_{\mathrm{M}}\left(\mathbf{C}_{\mathrm{V}}^{\mathrm{m},\mathcal{E}},\mathbf{C}_{\mathcal{E}}^{\mathrm{m}},\mathbf{C}_{\mathrm{V}}^{\mathrm{f},\mathcal{E}},\mathbf{C}_{\mathcal{E}}^{\mathrm{f}},\theta,\mathbf{A}_{0},\xi^{\mathrm{m}},\xi^{\mathrm{f}}\right)+\overline{\Psi}_{\theta}\left(\theta\right) \tag{42}$$

2.4.1. Thermal free energy function

The thermal contribution is defined as [34]:

$$\overline{\Psi}_{\theta}\left(\theta\right)=-\int_{\theta_{\mathrm{ref}}}^{\theta}\mathrm{C}_{\mathrm{vol}}\left(\hat{\theta}\right)\left(\theta-\hat{\theta}\right)\frac{\mathrm{d}\hat{\theta}}{\hat{\theta}} \tag{43}$$

where C_{vol} and θ_{ref} are the specific heat capacity at constant volume and the reference temperature.

2.4.2. Mechanical free energy function

The mechanical free energy function consists of the isotropic (matrix, $\overline{\Psi}_{\mathrm{M}}^{\mathrm{m}}$) and the anisotropic (fiber, $\overline{\Psi}_{\mathrm{M}}^{\mathrm{f}}$) parts:

$$\begin{aligned}\overline{\Psi}_{\mathrm{M}}\left(\mathbf{C}_{\mathrm{V}}^{\mathrm{i},\mathcal{E}},\mathbf{C}_{\mathcal{E}}^{\mathrm{i}},\theta,\mathbf{A}_{0},\xi^{\mathrm{m}},\xi^{\mathrm{f}}\right)&=\overline{\Psi}_{\mathrm{M}}^{\mathrm{m}}\left(\mathbf{C}_{\mathrm{V}}^{\mathrm{m},\mathcal{E}},\mathbf{C}_{\mathcal{E}}^{\mathrm{m}},\theta,\xi^{\mathrm{m}}\right)\\&+\overline{\Psi}_{\mathrm{M}}^{\mathrm{f}}\left(\mathbf{C}_{\mathrm{V}}^{\mathrm{f},\mathcal{E}},\mathbf{C}_{\mathcal{E}}^{\mathrm{f}},\theta,\mathbf{A}_{0},\xi^{\mathrm{f}}\right)\end{aligned} \tag{44}$$

Additionally, each parts of the mechanical free energy function involves pure elastic ($\overline{\Psi}_{\mathcal{E}}^{\mathrm{m}}$ and $\overline{\Psi}_{\mathcal{E}}^{\mathrm{f}}$ for matrix and fiber respectively) and viscous ($\overline{\Psi}_{\mathrm{V}}^{\mathrm{m}}$ and $\overline{\Psi}_{\mathrm{V}}^{\mathrm{f}}$ for matrix and fiber respectively) divisions. This method has been applied in another studies [56,57]. While the pure elastic response handles quasi-static (equilibrium) loads, the viscous contribution explains the rate dependency (non-equilibrium):

$$\overline{\Psi}_{\mathrm{M}}^{\mathrm{m}}\left(\mathbf{C}_{\mathrm{V}}^{\mathrm{m},\mathcal{E}},\mathbf{C}_{\mathcal{E}}^{\mathrm{m}},\theta,\xi^{\mathrm{m}}\right)=\overline{\Psi}_{\mathcal{E}}^{\mathrm{m}}\left(\mathbf{C}_{\mathcal{E}}^{\mathrm{m}},\theta,\xi^{\mathrm{m}}\right)+\overline{\Psi}_{\mathrm{V}}^{\mathrm{m}}\left(\mathbf{C}_{\mathrm{V}}^{\mathrm{m},\mathcal{E}},\theta,\xi^{\mathrm{m}}\right) \tag{45}$$

and

$$\overline{\Psi}_{\mathrm{M}}^{\mathrm{f}}\left(\mathbf{C}_{\mathrm{V}}^{\mathrm{f},\mathcal{E}},\mathbf{C}_{\mathcal{E}}^{\mathrm{f}},\theta,\mathbf{A}_{0},\xi^{\mathrm{f}}\right)=\overline{\Psi}_{\mathcal{E}}^{\mathrm{f}}\left(\mathbf{C}_{\mathcal{E}}^{\mathrm{f}},\theta,\mathbf{A}_{0},\xi^{\mathrm{f}}\right)+\overline{\Psi}_{\mathrm{V}}^{\mathrm{f}}\left(\mathbf{C}_{\mathrm{V}}^{\mathrm{f},\mathcal{E}},\theta,\mathbf{A}_{0},\xi^{\mathrm{f}}\right) \tag{46}$$

2.4.2.1. Isotropic response. The isotropic free energy function has been decoupled into pure elastic and viscous parts as stated earlier. The pure elastic is also related to isochoric ($\overline{\Psi}_{\mathcal{E}}^{\mathrm{m,ich}}$) and volumetric ($\overline{\Psi}_{\mathcal{E}}^{\mathrm{m,vol}}$) responses:

$$\overline{\Psi}_{\mathcal{E}}^{\mathrm{m}}\left(\mathbf{C}_{\mathcal{E}}^{\mathrm{m}},\theta,\xi^{\mathrm{m}}\right)=\overline{\Psi}_{\mathcal{E}}^{\mathrm{m,ich}}+\overline{\Psi}_{\mathcal{E}}^{\mathrm{m,vol}} \tag{47}$$

The first part depends on the pure elastic right Cauchy–Green tensor ($\mathbf{C}_{\mathcal{E}}^{\mathrm{m}}$), temperature ($\theta$) and matrix damage ($\xi^{\mathrm{m}}$). The other part depends

on the temperature and Jacobian $J_M = \det(\mathbf{F}_M)$ that presents volume change. As the majority of soft tissues are composed of water, they are usually assumed to be incompressible [22,58] and hence $\overline{\Psi}^{m,vol}_{\mathcal{E}}$ in Eq. (47) can be neglected.

The matrix damage parameter (ξ^m) is used to relate the undamaged ($\tilde{\Psi}^m_{\mathcal{E}}$) and damaged ($\overline{\Psi}^m_{\mathcal{E}}$) energy functions:

$$\overline{\Psi}^m_{\mathcal{E}}\left(\mathbf{C}^m_{\mathcal{E}}, \theta, \xi^m\right) = \left(1-\xi^m\right)\tilde{\Psi}^m_{\mathcal{E}}\left(\mathbf{C}^m_{\mathcal{E}}, \theta\right) \tag{48}$$

To take into account the temperature effect, the temperature-dependent Ogden model is selected [34]:

$$\tilde{\Psi}^m_{\mathcal{E}} = \sum_{j=1}^{\infty} \frac{\mu_j(\theta)}{\alpha_j}\left(\lambda_{1,\mathcal{E}}{}^{\alpha_j} + \lambda_{2,\mathcal{E}}{}^{\alpha_j} + \lambda_{3,\mathcal{E}}{}^{\alpha_j} - 3\right) \tag{49}$$

where $\mu_j(\theta) = \mu_j\left(\theta_{ref}\right) + \eta^m\left(\theta - \theta_{ref}\right)$ and μ_j, η^m, α are material parameters and θ_{ref} is the reference temperature. In this equation $\lambda_{i,\mathcal{E}}(i = 1,2,3)$ are the elastic principal stretches of the isochoric part. The material parameters of the Ogden model should satisfy the $\mu_j\alpha_j \geq 0$ condition [59].

Also, the matrix viscous response, $\overline{\Psi}^m_V$ which is related to the elastic part of viscous right Cauchy–Green tensor ($\mathbf{C}^{m,\mathcal{E}}_V$), temperature and matrix damage, can be obtained with a similar manner [24]:

$$\overline{\Psi}^m_V\left(\mathbf{C}^m_{\mathcal{E}}, \theta, \xi^m\right) = \left(1-\xi^m\right)\tilde{\Psi}^m_V\left(\mathbf{C}^{m,\mathcal{E}}_V, \theta\right) \tag{50}$$

Substituting the elastic principal stretches of the viscous response $\lambda^{\mathcal{E}}_{i,V}(i = 1,2,3)$:

$$\tilde{\Psi}^m_V = \sum_{j=1}^{\infty} \frac{\mu_j^V(\theta)}{\alpha_j^V}\left(\lambda^{\mathcal{E}}_{1,V}{}^{\alpha_j^V} + \lambda^{\mathcal{E}}_{2,V}{}^{\alpha_j^V} + \lambda^{\mathcal{E}}_{3,V}{}^{\alpha_j^V} - 3\right) \tag{51}$$

where $\mu_j^V(\theta) = \mu_j^V\left(\theta_{ref}\right) + \eta^m\left(\theta - \theta_{ref}\right)$. In this relation μ^V, η^m and α^V are material properties.

2.4.2.2. Anisotropic response. The anisotropic energy function ($\overline{\Psi}^f_M$) is also decoupled into the pure elastic ($\overline{\Psi}^f_{\mathcal{E}}$) and viscous ($\overline{\Psi}^f_V$) parts in a similar method. The undamaged elastic ($\tilde{\Psi}^f_{\mathcal{E}}$) and the viscous responses ($\tilde{\Psi}^f_V$) are affected by damage of fiber ξ^f as:

$$\overline{\Psi}^f_{\mathcal{E}}\left(\mathbf{C}^f_{\mathcal{E}}, \theta, \mathbf{A}_0, \xi^f\right) = \left(1-\xi^f\right)\tilde{\Psi}^f_{\mathcal{E}} \tag{52}$$

$$\overline{\Psi}^f_V\left(\mathbf{C}^{f,\mathcal{E}}_V, \theta, \mathbf{A}_0, \xi^f\right) = \left(1-\xi^f\right)\tilde{\Psi}^f_V \tag{53}$$

where $\mathbf{C}^f_{\mathcal{E}}$ is fiber's pure elastic right Cauchy–Green tensor and $\mathbf{C}^{f,\mathcal{E}}_V$ is elastic part of fiber's viscous right Cauchy–Green tensor.

The temperature-independent function for elastic part is the one proposed by Gasser et al. [14]. This function is improved by considering the martial parameters as temperature dependent, hence, a new term showing the temperature effect is added:

$$\tilde{\Psi}^f_{\mathcal{E}}\left(\mathbf{C}^f_{\mathcal{E}}, \theta, \mathbf{A}_0\right) = \begin{cases} \dfrac{k_1(\theta)}{2k_2}\left[e^{k_2\left(I^{*f}_{4,\mathcal{E}}-1\right)^2} - 1\right] & \text{if } I^{*f}_{4,\mathcal{E}} > 0 \\ 0 & \text{otherwise} \end{cases} \tag{54}$$

where $k_1(\theta) = k_1\left(\theta_{ref}\right) + \eta^f\left(\theta - \theta_{ref}\right)$, in which k_1, η^f and k_2 are material parameters and $I^{f,ich}_{4,\mathcal{E}}$ is the isochoric fourth strain invariant that depends on the elastic right Cauchy–Green deformation tensor $\mathbf{C}^f_{\mathcal{E}}$:

$$I^{f,ich}_{4,\mathcal{E}} = J_M^{-2/3}\boldsymbol{a}_0 \otimes \boldsymbol{a}_0 : \mathbf{C}^f_{\mathcal{E}}$$

Also,

$$\tilde{\Psi}^f_V\left(\mathbf{C}^{f,\mathcal{E}}_V, \theta, \mathbf{A}_0\right) = \begin{cases} \dfrac{k_1^v(\theta)}{2k_2^v}\left[e^{k_2^v\left(I^{f,ich}_{4,\mathcal{E}}-1\right)^2} - 1\right] & \text{if } I^{f,ich}_{4,\mathcal{E}} > 0 \\ 0 & \text{otherwise} \end{cases} \tag{55}$$

where $k_1^v(\theta) = k_1^v\left(\theta_{ref}\right) + \eta^f\left(\theta - \theta_{ref}\right)$, in which k_1^v, η^f and k_2^v are material parameters and $I^{f,ich}_{4,\mathcal{E}}$ is the isochoric fourth strain invariant that depends on the viscous right Cauchy–Green deformation tensor $\mathbf{C}^{f,\mathcal{E}}_V$.

The viscous deformation gradient $\mathbf{F}^{i,v}_V$ and damage characterize the history dependent effects. To complete the constitutive description, the evolutions of these internal state variables must be specified constitutively.

2.4.3. Viscous flow rule

The viscous flow rule is used to evaluate $\mathbf{F}^{i,v}_V$ [60]:

$$\bar{\mathbf{l}}^{i,v,ich}_V = \dot{\mathbf{F}}^{i,v,ich}_V\mathbf{F}^{-i,v,ich}_V = \dot{\gamma}^{i,v}\mathbf{N}^{i,v} \qquad i = m \text{ and } f \tag{56}$$

where $\dot{\gamma}^{i,v}$ is the accumulated viscous strain rate and $\mathbf{N}^v$ is the direction tensor of viscous flow:

$$\mathbf{N}^{i,v} = \frac{\boldsymbol{\sigma}^{i,dev}_V}{\left\|\boldsymbol{\sigma}^{i,dev}_V\right\|} = \frac{\boldsymbol{\sigma}^{i,dev}_V}{\sqrt{tr\left(\boldsymbol{\sigma}^{i,dev}_V\boldsymbol{\sigma}^{i,dev}_V\right)}} \qquad i = m \text{ and } f \tag{57}$$

Here $\boldsymbol{\sigma}^{i,dev}_V$ is the deviatoric part of the Cauchy stress tensor and $\left\|\boldsymbol{\sigma}^{i,dev}_V\right\|$ is the effective viscous flow stress by the Frobenius norm. Many studies consider the viscous strain rate as a function of effective viscous flow stress [61,62]:

$$\dot{\gamma}^{i,v} = \dot{\gamma}^{i,v}\left(\left\|\boldsymbol{\sigma}^{i,dev}_V\right\|\right) \qquad i = m \text{ and } f \tag{58}$$

$$\dot{\gamma}^{i,v} = \dot{\gamma}^{i,v}_0\left|\lambda^{i,v}_V - 1 + \zeta^i\right|^{n^i}\left(\frac{\left\|\boldsymbol{\sigma}^{i,dev}_V\right\|}{\tau^i_0}\right)^{z^i}\left(\frac{\theta}{\theta_{ref}}\right)^{\delta^i} \qquad i = m \text{ and } f \tag{59}$$

where $\dot{\gamma}^{i,v}_0$, ζ^i, τ^i_0, z^i, n^i and δ^i are material parameters and $\lambda^{i,v}_V$ is the viscous stretch:

$$\lambda^{i,v}_V = \sqrt{\frac{1}{3}tr\left(\mathbf{F}^{i,v,ich}_V\mathbf{F}^{i,v,ich,T}_V\right)} \qquad i = m \text{ and } f \tag{60}$$

in which $\mathbf{F}^{i,v,ich}_V$ is the isochoric part of $\mathbf{F}^{i,v}_V$.

2.4.4. Rate dependent damage

According to the formulation, it is necessary to calculate the damage at each stage. Equations for damage evolution must satisfy some important conditions which are given by Peña [63]. In the majority of studies, the damage criterion is defined based on the distortional (isochoric) energy ($\tilde{\Psi}^{i,ich}$) as [35,64,65]:

$$\varphi^i = \sqrt{2\tilde{\Psi}^{i,ich}\left(\mathbf{C}^i(t)\right)} - p^i_t = \Xi^i_t - p^i_t \leq 0 \qquad i = m \text{ and } f \tag{61}$$

where p^i_t is the damage threshold at the current time [64]. With respect to Eq. (61), $\varphi^i = 0$ defines the outer boundary of the undamaged volume.

Damage evolution has an irreversible rate equation as [64]:

$$\frac{d\xi^i}{dt} = \chi^i\left\langle\Gamma\left(\varphi^i\right)\right\rangle\bar{h}^i\left(\Xi^i_t, \xi^i\right) \qquad i = m \text{ and } f \tag{62}$$

$$\frac{dp^i_t}{dt} = \chi^i\left\langle\Gamma\left(\varphi^i\right)\right\rangle = \chi^i\left\langle\Gamma\left(\Xi^i_t - p^i_t\right)\right\rangle \qquad i = m \text{ and } f \tag{63}$$

where χ is the damage viscosity coefficient, $\langle\cdot\rangle$ denotes the Macaulay bracket, $\Gamma\left(\varphi^i\right)$ is the viscous damage flow function and $\bar{h}^i$ is the damage evolution function. Linear viscous damage can be considered as $\Gamma\left(\varphi^i\right) = \varphi^i$ and $\dot{p}^i_t = \chi^i\varphi^i$ [64,65]. It is common to assume $\bar{h}^i$ to be independent of ξ^i [35,65]. Damage can be evaluated using an exponential function [65]:

$$\bar{h}^i = a^ib^i\exp\left[a^i\left(\Xi^i_0 - \Xi^i_t\right)\right] \qquad i = m \text{ and } f \tag{64}$$

where a^i and b^i are material parameters and Ξ^i_0 denotes the characteristic initial damage threshold for matrix and fiber. In this study, we couple damage with temperature using an Arrhenius-type temperature term as:

$$\bar{h}^i\left(\Xi^i_t, \theta\right) = \bar{h}^i\left(\Xi^i_t\right)\exp\left(-\frac{\theta_{ref}}{\theta}\right) \qquad i = m \text{ and } f \tag{65}$$

where θ_{ref} is the reference temperature.

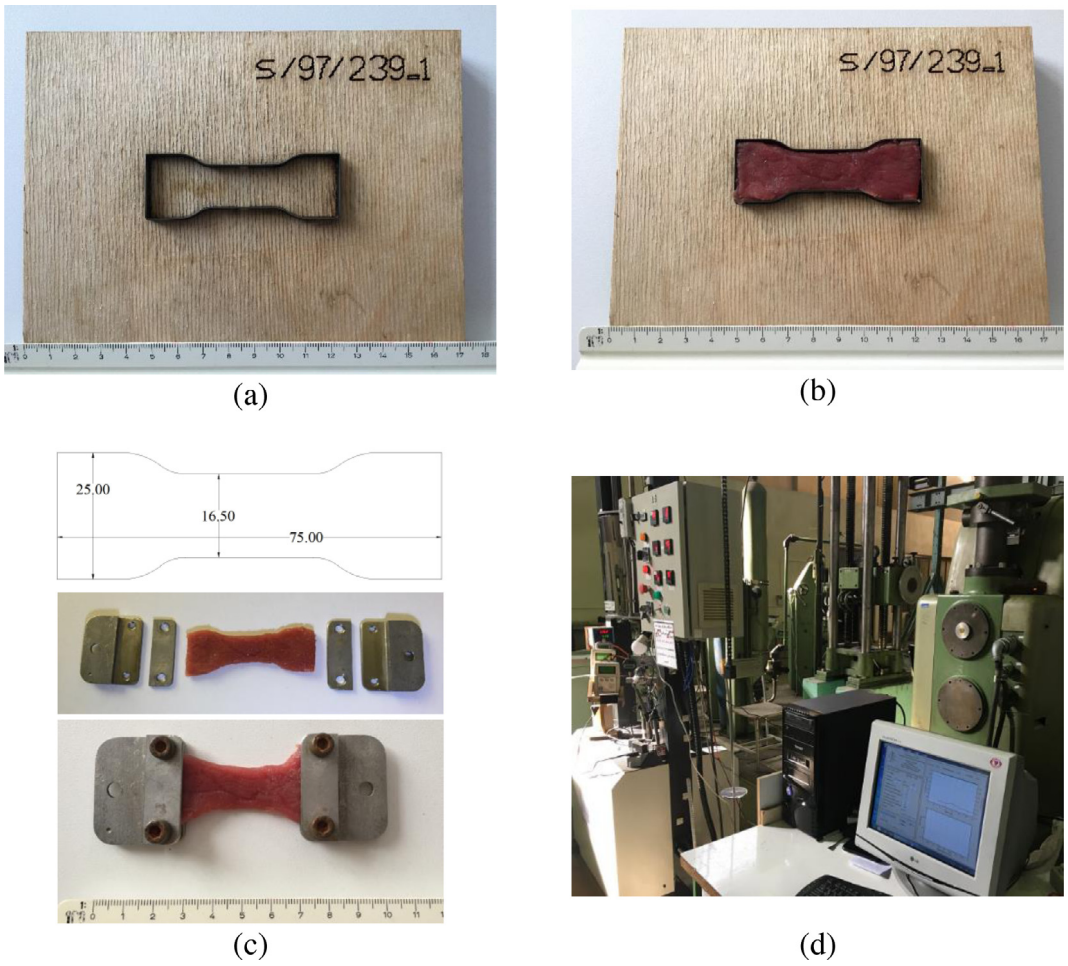

Fig. 3. Sample preparation and experimental setup.

3. Numerical solution method

The developed model can be employed to predict the fibrous soft tissue's temperature and rate dependent behavior. For this purpose, solving the described equations is essential. Firstly, we calculate the material parameters of these equations using a metaheuristic optimization technique. We also obtain experimental data using a set of uniaxial cyclic tests on bovine round muscle. In the following, we explain the solution method for the uniaxial form of the model.

3.1. Uniaxial solution algorithm

The solution steps can be employed in an incremental approach:

1. Initial deformation gradient, temperature and damage are known/measured (initial conditions);
2. Calculate elastic and viscous stresses at t_n using Eqs. (31) and (32) (See Appendix for the uniaxial solution);
3. Using an ODE solver to solve Eqs. (56), (57) and (59), calculate $\mathbf{F}_V^{i,v}$ at t_{n+1}. In this paper, we use the Runge–Kutta method [66].
4. Calculate $\Xi^i_{t_{n+1}} = \sqrt{2\tilde{\Psi}^{i,ich}\left(\mathbf{C}^i\left(t_{n+1}\right)\right)}$ $\quad i = m \text{ and } f;$
5. Check damage criterion $\varphi^i_{t_{n+1}} = \Xi^i_{t_{n+1}} - p^i_t$ $\quad i = m \text{ and } f:$

   5.1. If $\varphi^i > 0$ (damage is taking place) then update damage parameters employing equations (62), (63) and (65). For this purpose, Ju [64] proposed the backward Euler finite difference method:

$$\Delta\chi^i_{t_{n+1}} = \chi^i\left(t_{n+1} - t_n\right) \quad i = m \text{ and } f \tag{66}$$

Table 1
Thermal material properties tissue [69].

θ (°C)	25	30	35	40	45
$C_{vol}\left(\frac{J}{kg\,°C}\right)$	3627	3629	3631	3634	3637
$\alpha_\theta\left(\frac{1}{°C}\right)$	2.4×10^{-4}	2.6×10^{-4}	2.9×10^{-4}	3.2×10^{-4}	3.4×10^{-4}

$$p^i_{t_{n+1}} = \frac{p^i_{t_n} + \Delta\chi^i_{t_{n+1}}\Xi^i_{t_{n+1}}}{1 + \Delta\chi^i_{t_{n+1}}} \quad i = m \text{ and } f \tag{67}$$

$$\xi^i_{t_{n+1}} = \xi^i_{t_n} + \Delta\chi^i_{t_{n+1}}\varphi^i_{t_{n+1}}\bar{h}^i_{t_{n+1}} \quad i = m \text{ and } f \tag{68}$$

   5.2. If $\varphi^i \le 0$ then:

$$\xi^i_{t_{n+1}} = \xi^i_{t_n} \quad i = m \text{ and } f \tag{69}$$

6. Calculate $\bar{\eta}$ and $\dot{\bar{\eta}}$ using Eqs. (33) and (38). For this aim, we take the thermal constants presented in Table 1.
7. Calculate intrinsic dissipation ($\overline{D}_I$) employing equation (35);
8. Solve partial differential equation (39) for $\theta_{t_{n+1}}$ distribution. In this paper, we use a combination of the backward finite difference and the four stage Lobatto IIIA formula [67]. Also, we take the conductivity coefficient to be equal to 0.4 W/m K [68].

Table 2
Samples description and case study numbers (Part (a) are used to obtain the constitutive parameters; Part (b) and (c) are used to validate the results).

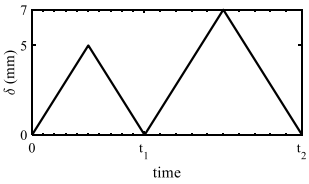

Loading Pattern (displacement vs. time)

		Fibers Angel $\beta = 90^o$		Fibers Angel $\beta = 0^o$	
		$\dot{\varepsilon} = 2 \times 10^{-4}$ 1/s	$\dot{\varepsilon} = 2 \times 10^{-3}$ 1/s	$\dot{\varepsilon} = 2 \times 10^{-4}$ 1/s	$\dot{\varepsilon} = 2 \times 10^{-3}$ 1/s
	T = 25 °C	**N25R1**	**N25R2**	**P25R1**	**P25R2**
(a)	T = 35 °C	**N35R1**	–	**P35R1**	–
	T = 45 °C	**N45R1**	–	**P45R1**	–

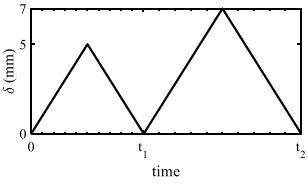

Loading Pattern (displacement vs. time)

		Fibers Angel $\beta = 90^o$ $\dot{\varepsilon} = 2 \times 10^{-3}$ 1/s	Fibers Angel $\beta = 0^o$ $\dot{\varepsilon} = 2 \times 10^{-3}$ 1/s
(b)	T = 35 °C	**VN35R2**	**VP35R2**
	T = 45 °C	**VN45R2**	**VP45R2**

		Tensile Test
		Fibers Angel $\beta = 90^o$ $\dot{\varepsilon} = 1.8 \times 10^{-2}$ 1/s
(c)	T = 25 °C	**VP25Tensile**

Table 3
Characteristics of the GA.

GA type	Continuous
Population size	30
Mutation rate	0.2
Pairing method	Rank weighting
Selection rate	0.5

3.2. Obtaining constitutive parameters using the genetic algorithm

As a metaheuristic technique, we develop the well-known continuous Genetic Algorithm (GA) to calculate the 28 unknown material parameters in the model. This method was successfully used previously for determining the material properties in tissues [70–72]. Based on the natural evolution, GA optimizes the initial random population of material parameters by a proper selecting rule.

In the first step, GA generates an initial random population. In the next action, the objective function (O) is evaluated and data are sorted based on their fitness. In this paper, the objective function is defined using the least square error between the experimental data ($\boldsymbol{\sigma}^{\mathrm{Exp}}$) and model predictions ($\boldsymbol{\sigma}^{\mathrm{Model}}$):

$$\mathrm{O} = \sqrt{\frac{1}{\mathrm{N}} \sum_{\mathrm{j}=1}^{\mathrm{N}} \left(\frac{\int_0^{\mathrm{t_{end,j}}} \left\| \boldsymbol{\sigma}_{\mathrm{j}}^{\mathrm{Model}} - \boldsymbol{\sigma}_{\mathrm{j}}^{\mathrm{Exp}} \right\| \mathrm{dt}}{\max \left\| \boldsymbol{\sigma}_{\mathrm{j}}^{\mathrm{Exp}} \right\|} \right)^2} \tag{70}$$

where N is the total number of experiments used to obtain constitutive parameters, $\mathrm{t_{end,j}}$ is time at the end of each experiment and $\|\cdot\|$ denotes the Euclidean norm. Also:

Table 4
Calculated biomechanical properties for (a) Matrix and (b) Fibers of bovine round muscle.

(a)	μ (kPa)	α	μ^{v} (kPa)	α^{v}	η^{m} ($\frac{\mathrm{kPa}}{\mathrm{K}}$)	δ^{m}	$\dot{\gamma}_0^{\mathrm{m,v}}$ (s^{-1})
	27.00	5.80	96.00	2.50	−800	1.70	0.59
	z^{m}	n^{m}	τ_0^{m} (MPa)	ζ^{m}	b^{m}	χ^{m}	a^{m}
	1.20	1.60	5.40	0.55	2.60	1000	2.40
(b)	k_1 (kPa)	k_2	k_1^{v} (kPa)	k_2^{v}	η^{f} ($\frac{\mathrm{kPa}}{\mathrm{K}}$)	δ^{f}	$\dot{\gamma}_0^{\mathrm{f,v}}$ (s^{-1})
	28.00	0.87	120.00	6.40	−300	3.00	0.64
	z^{f}	n^{f}	τ_0^{f} (MPa)	ζ^{f}	b^{f}	χ^{f}	a^{f}
	0.39	0.62	370.00	0.79	5.90	99	8.92

$$\boldsymbol{\sigma}^{\mathrm{Model}} = \boldsymbol{\sigma}^{\mathrm{m}} + \boldsymbol{\sigma}^{\mathrm{f}} = \mathrm{J_M F_M} \left(\overline{\mathbf{S}}_{\mathcal{E}}^{\mathrm{m}} + \overline{\mathbf{S}}_{\mathrm{V}}^{\mathrm{m}} + \overline{\mathbf{S}}_{\mathcal{E}}^{\mathrm{f}} + \overline{\mathbf{S}}_{\mathrm{V}}^{\mathrm{f}} \right) \mathbf{F}_{\mathrm{M}}^{\mathrm{T}} \tag{71}$$

$$\boldsymbol{\sigma}^{\mathrm{Exp}} = \begin{bmatrix} \dfrac{\mathrm{Force^{Exp}}}{\mathrm{Area_0}} \left(1 + \dfrac{\Delta \mathrm{L^{exp}}}{\mathrm{L_0}} \right) & 0 & 0 \\ 0 & 0 & 0 \\ 0 & 0 & 0 \end{bmatrix} \tag{72}$$

in which $\mathrm{Force^{Exp}}$, $\mathrm{Area_0}$, $\mathrm{L_0}$ and $\Delta \mathrm{L^{exp}}$ are the force, initial cross-sectional area, initial length and change in the length respectively all measured during the tests.

Later, GA eliminates the inappropriate half of the population members. Among the surviving members, the algorithm chooses parents who will generate new data. We adopt the rank weighting technique

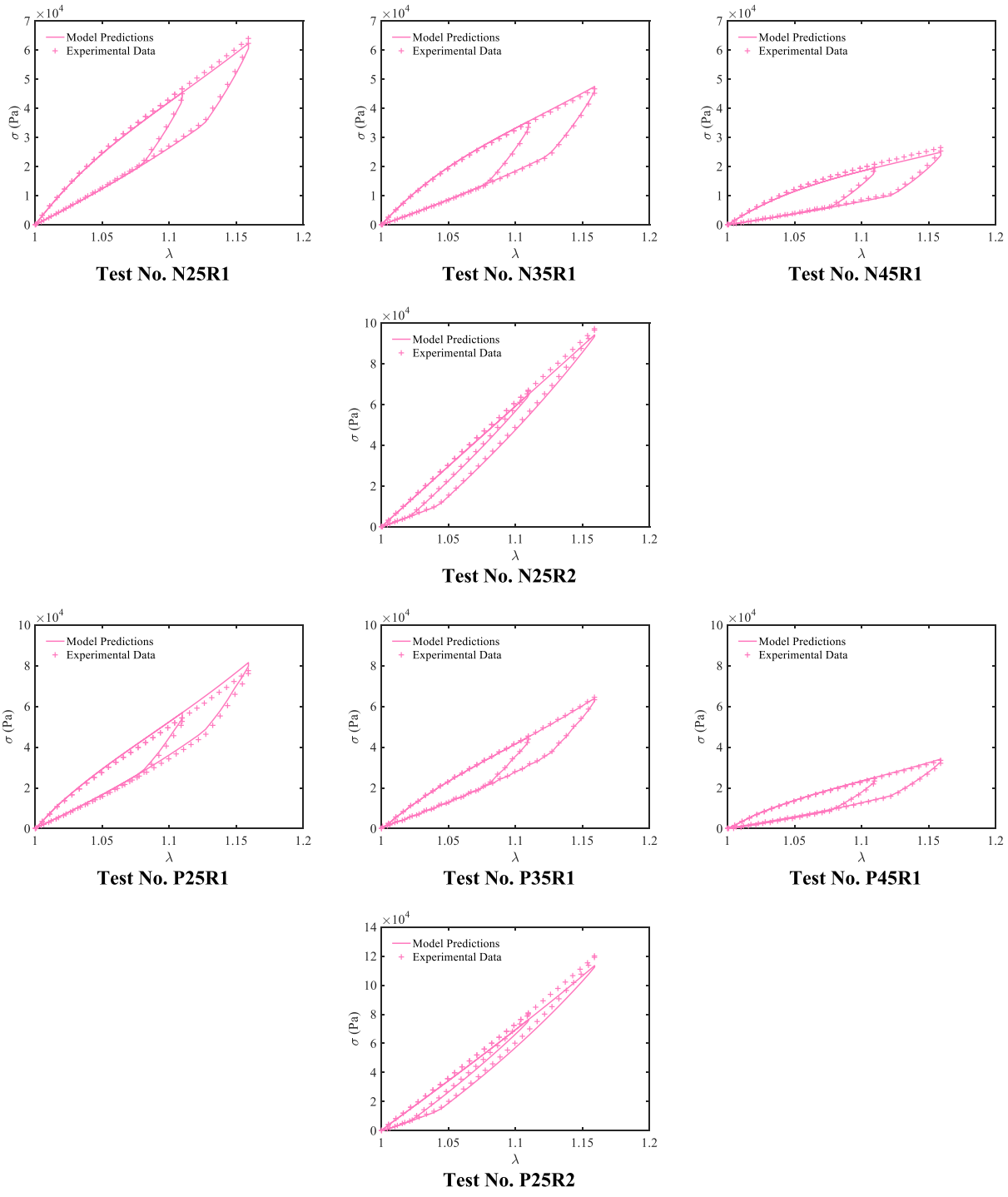

Fig. 4. Experimental cyclic tension test results vs. model predictions.

in which selecting depends on the rank probability (P_n) [73]:

$$P_n = \frac{\frac{N_{pop}}{2} - n + 1}{\sum_{n=1}^{\frac{N_{pop}}{2}} n} \tag{73}$$

where N_{pop} is the population size. Each parent pair produces two new members with continuous crossover operator; therefore, N_{pop} remains fixed. Our next move is to apply the mutation operator and evaluate the value of the objective function for the new members [73]. The above steps have been repeated until the solution converged. The GA parameters are defined in the results section.

4. Experimental procedure

A set of 39 uniaxial tensile cyclic experiments are performed at different levels of temperature and strain rates, parallel and normal to the tissue's fiber. For this purpose, in this study, we used bovine muscle because of its consistent muscle fiber orientation [74,75]. The temperature levels are 25 °C, 35°C, and 45 °C. Also, the strain rates are 0.02% mm/mm/s and 0.2% mm/mm/s. The temperature levels are selected based on the range of temperature used in the hyperthermia procedure.

Slices of test tissues were cut with a thickness of 5 mm using a predesigned fixture. Then, we punched samples by the mold (Fig. 3a)

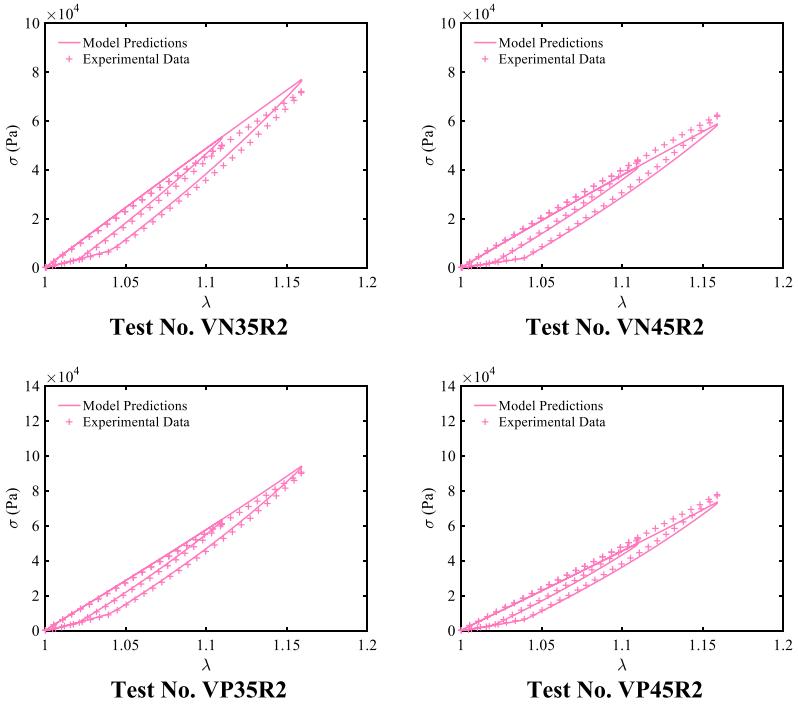

Fig. 5. Validating results (experimental cyclic tension test results vs. model predictions).

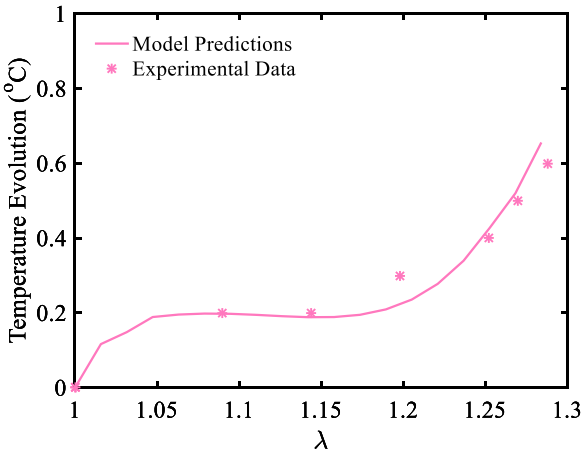

Fig. 6. Temperature evolution with stretch ratio predicted using developed model and experimental measurements; Initial temperature = 25 °C , strain rate = 1.8% s^{-1} and loading direction parallel to the fibers.

into a dog bone shape (Fig. 3b) to minimize the end effects due to the clamping force. The punches were done parallel to the tissue's fiber ($\beta = 0°$) and normal to them ($\beta = 90°$). We used a bio-bath of saline solution to prevent dehydration at high-temperature levels. The experiments were performed employing a uniaxial tensile testing machine. The specimens were mounted between two predesigned clamps (Fig. 3c) and then connected to the testing machine (Fig. 3d). Each test was repeated three times.

Table 2 summarizes the test conditions and loading pattern for each sample. The resultant load and displacement data of the samples were used to calculate stress and stretch ratio (the average values of initial length (L_0) and cross-sectional area ($Area_0$) were 45.0 mm and 62.5 mm^2 respectively; Eq. (72)).

Also, to validate the temperature variation predicted by solving Eq. (39), we carried out a tensile test is carried out at 25 °C and with the strain rate of 1.8% mm/mm/s. Temperature elevation during the test was measured and compared to the calculated values.

5. Results

5.1. Experimental results and obtaining constitutive parameters

As mentioned before, experiments have been done in different test conditions (Table 2). The output of each experiment is a load–displacement variation diagram. These results are divided into two parts. The results of the first set of tests are introduced to the GA code to determine the material properties of the model (Table 2(a)) and the results of the second set is used to validate the results (Table 2(b) and (c)). Table 3 defines the characteristics of the GA. The calculated material parameters are listed in Table 4. Fig. 4 compares the model prediction and the experimental results used to determine the material properties.

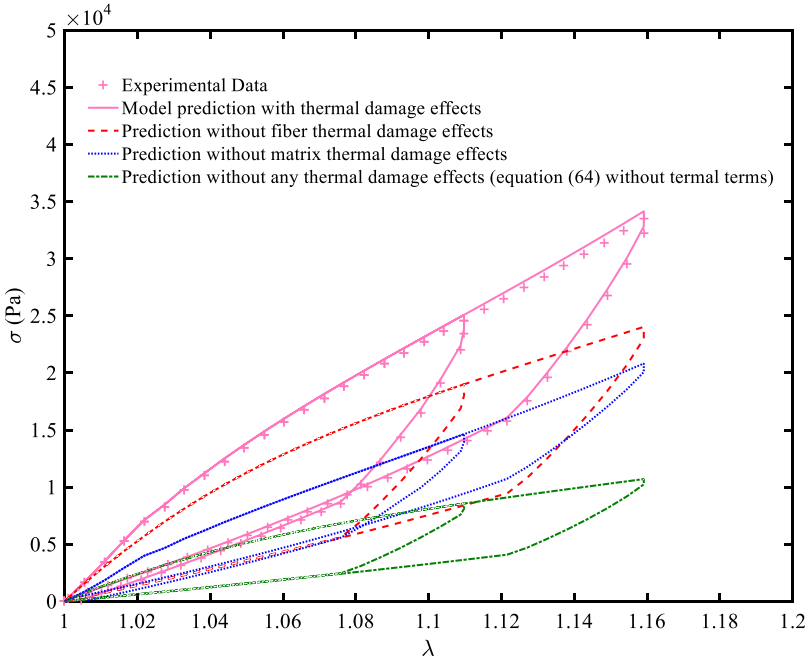

Fig. 7. Experimental cyclic tension test results vs. predictions with and without the thermal damage effect.

5.2. Model validation

As mentioned before, experimental data are divided into two parts. Those categorized in Table 2(a) are used to obtain the material parameters; while the second category (Table 2(b)) is employed to validate the model predictions. The model stress–stretch predictions and the experimental results are compared in Fig. 5. It can be seen that there is good agreement between experimental data and the model predictions with a maximum error of 6.72%:

$$\text{Error} = \frac{\left\|\boldsymbol{\sigma}^{\text{Model}} - \boldsymbol{\sigma}^{\text{Exp}}\right\|}{\left\|\boldsymbol{\sigma}^{\text{Exp}}\right\|} \times 100\% \tag{74}$$

The sources of this error can be divided in three reasons: (I) slight randomness of the fiber directions and fiber's homogeneity, (II) accuracy of the measuring equipment and (III) compromise in the optimization technique.

According to the TVHD coupling partial differential equation (Eq. (39)), mechanical effects will cause temperature change in the tissue. To investigate the capability of the developed model to predict this effect, the temperature rise of a sample in a tensile test is measured and compared to the model predictions (Fig. 6). This experiment is carried out with $\beta = 0°$ and $\dot{\varepsilon} = 1.8\%$ mm/mm/s. It can be seen that there is good agreement between the calculated results and test data.

5.3. Discussion

In this section we study the effect of different parameters including the strain rate and the sample initial temperature. Figs. 4 and 5 reflect the effect of strain rate and temperature on the stress–stretch behavior of the tissue. These figures show that by increasing the temperature level and/or decreasing the strain rate, the tissue softens and deforms with lower applied stress levels. For example, at $\dot{\varepsilon} = 2 \times 10^{-4}$ 1/s, by increasing the temperature from 25 °C to 45 °C (cases studies N25R1 and N45R1) the required stress to stretch the tissue to $\lambda = 1.16$, reduces from 62.3 to 47.5 kPa. On the other hand, at 25 °C, by increasing the strain rate from 2×10^{-4} 1/s to 2×10^{-3} 1/s, the required stress to stretch the tissue to $\lambda = 1.16$, increases from 62.3 to 94.2 kPa.

Also, these figures show the stress–stretch behavior for the tissues with different fiber directions: $\beta = 0°$ and $\beta = 90°$. The results show that when the loading direction is normal to the fibers, the tissue behaves softly. In other words, the required stress to stretch the tissue reduces significantly. For example, at $\dot{\varepsilon} = 2 \times 10^{-4}$ 1/s and 25°C, by changing the load direction from $\beta = 0°$ and $\beta = 90°$, (cases studies N25R1 and P25R1) the required stress to stretch the tissue to $\lambda = 1.16$, increases from 62.3 to 81.6 kPa.

To demonstrate the importance of the thermal damage effects, Fig. 7 presents results based on the existing damage model without or with thermal effects in terms of one tensile test results (Case P45R1). The maximum error with thermal damage effects is 1.96%, and this figure shows that ignoring thermal effects on the fiber and matrix will increase the error to 28.25% and 37.81% respectively. Ignoring the thermal effects on both matrix and fiber damage which is Peña's model [65] in the form of Eq. (64), produces a 68.03% error compared with the experimental data. Additionally, the results show that the thermal damage effect on the matrix is more significant than the fiber.

Fig. 8 represents the isochronous stress contours with the initial temperature and strain rate. As can be seen, when the direction of the load is parallel with fibers, the stress is more dependent on the strain rate and temperature. Also, at high strain rates, stress variation with temperature is approximately steady.

To illustrate the effect of the coupled TVHD model, Fig. 9 represents the temperature elevation contours at $\lambda = 1.25$ concerning the initial temperature and strain rate. This figure shows that the temperature elevation depends on the initial temperature and strain rate. Based on these contours, at high temperature or strain rates, the error in calculating the temperature level ($\frac{\Delta\theta}{\theta_0}$) increases. For example, at 40 °C and $\dot{\varepsilon} = 0.015$ mm/mm/s, error in the uncoupled model increases to 5%. Also, under 0.005 mm/mm/s, error will be less than 2%. Assuming the quasi-static behavior for loadings with strain rates between 10^{-5} to 10^{-1} mm/mm/s, the results show that it is necessary to employ the coupled TVHD model to obtain more accurate results, especially in high strain rates. It is because lower temperature elevations are critical in soft tissues compared to the other materials.

6. Conclusions

A coupled thermo-visco-hyperelastic damage (TVHD) model is developed to predict the behavior of soft fibrous tissues. Also, the constitutive parameters of the model are obtained using the experimental

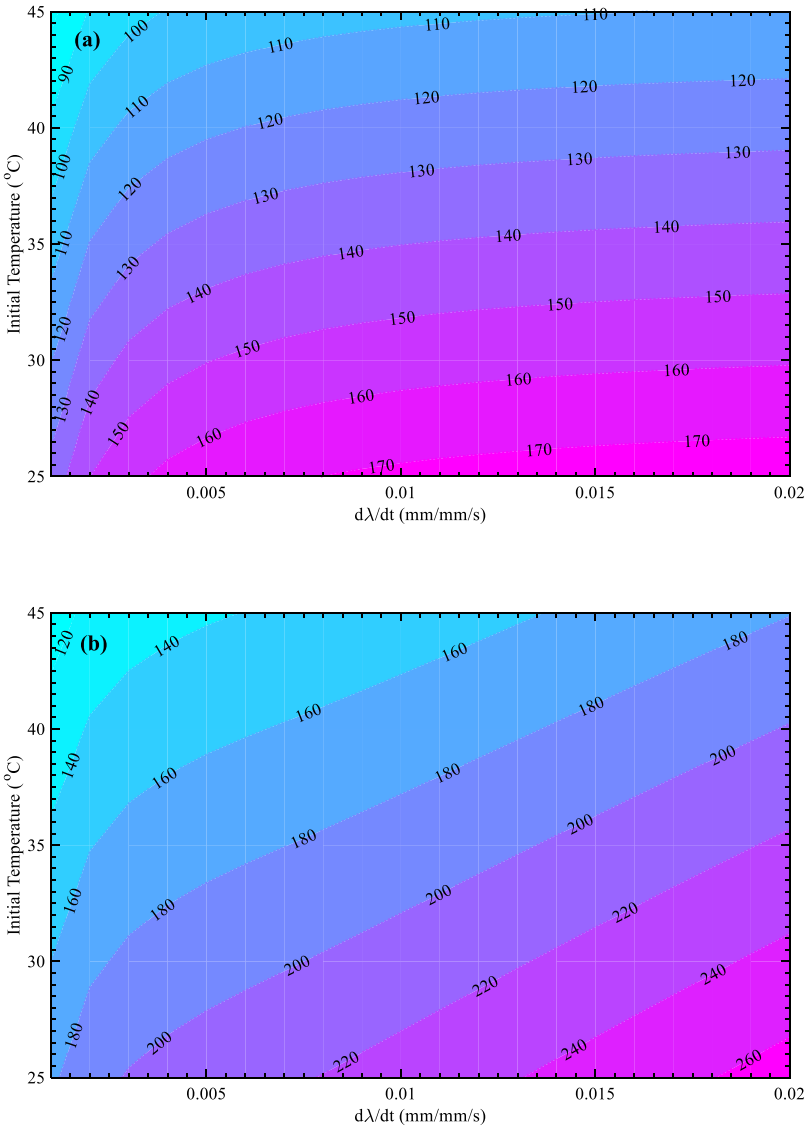

Fig. 8. Initial temperature–strain rate map with isochronous stress (kPa) contours for loading directions of (a) normal and (b) parallel to the fibers at $\lambda = 1.25$.

data and genetic algorithm based optimization technique. The results show that:

- Comparison of the experimental data and model predictions, reveals that it is necessary to use the developed coupled TVHD model to obtain more accurate results.
- At high strain rate and temperature levels, the temperature change due to the coupled thermo-mechanical effects is more significant. This is more important for the loadings which are parallel to the fibers.
- Not only it is essential to use the coupled TVHD model, but also, including the thermal damage effects considerably reduces the error of the predictions (from 68.03% to 1.96% in one case study).
- The thermal damage effect is more dominant in the matrix than the fiber of the tissue.
- The stress in the direction of the fibers is more dependent on the strain rate and temperature.

Acknowledgments

We declare that we have no financial or personal relationships with other people or organizations that could inappropriately influence our work.

Appendix. Uniaxial stress solution

For the uniaxial test, mechanical deformation gradient can be assumed as follows:

$$\mathbf{F}_{\mathrm{M}} = \begin{bmatrix} \lambda_1 & 0 & 0 \\ 0 & \lambda_2 & 0 \\ 0 & 0 & \lambda_3 \end{bmatrix} \tag{A.1}$$

As mentioned before, soft tissue is supposed to be incompressible and according to the Jacobian determinants the constraint $\lambda_1\lambda_2\lambda_3 = 1$ should be satisfied. Considering that $\lambda_2 = \lambda_3$:

$$\mathbf{F}_{\mathrm{M}}^{\mathrm{i}} = \begin{bmatrix} \lambda_{\mathcal{E}}^{\mathrm{i}} & 0 & 0 \\ 0 & \dfrac{1}{\sqrt{\lambda_{\mathcal{E}}^{\mathrm{i}}}} & 0 \\ 0 & 0 & \dfrac{1}{\sqrt{\lambda_{\mathcal{E}}^{\mathrm{i}}}} \end{bmatrix} = \begin{bmatrix} \lambda_{\mathrm{V}}^{\mathrm{i},\mathcal{E}} & 0 & 0 \\ 0 & \dfrac{1}{\sqrt{\lambda_{\mathrm{V}}^{\mathrm{i},\mathcal{E}}}} & 0 \\ 0 & 0 & \dfrac{1}{\sqrt{\lambda_{\mathrm{V}}^{\mathrm{i},\mathcal{E}}}} \end{bmatrix} \times \begin{bmatrix} \lambda_{\mathrm{V}}^{\mathrm{i,v}} & 0 & 0 \\ 0 & \dfrac{1}{\sqrt{\lambda_{\mathrm{V}}^{\mathrm{i,v}}}} & 0 \\ 0 & 0 & \dfrac{1}{\sqrt{\lambda_{\mathrm{V}}^{\mathrm{i,v}}}} \end{bmatrix} \mathrm{i} = \mathrm{m} \text{ and } \mathrm{f} \tag{A.2}$$

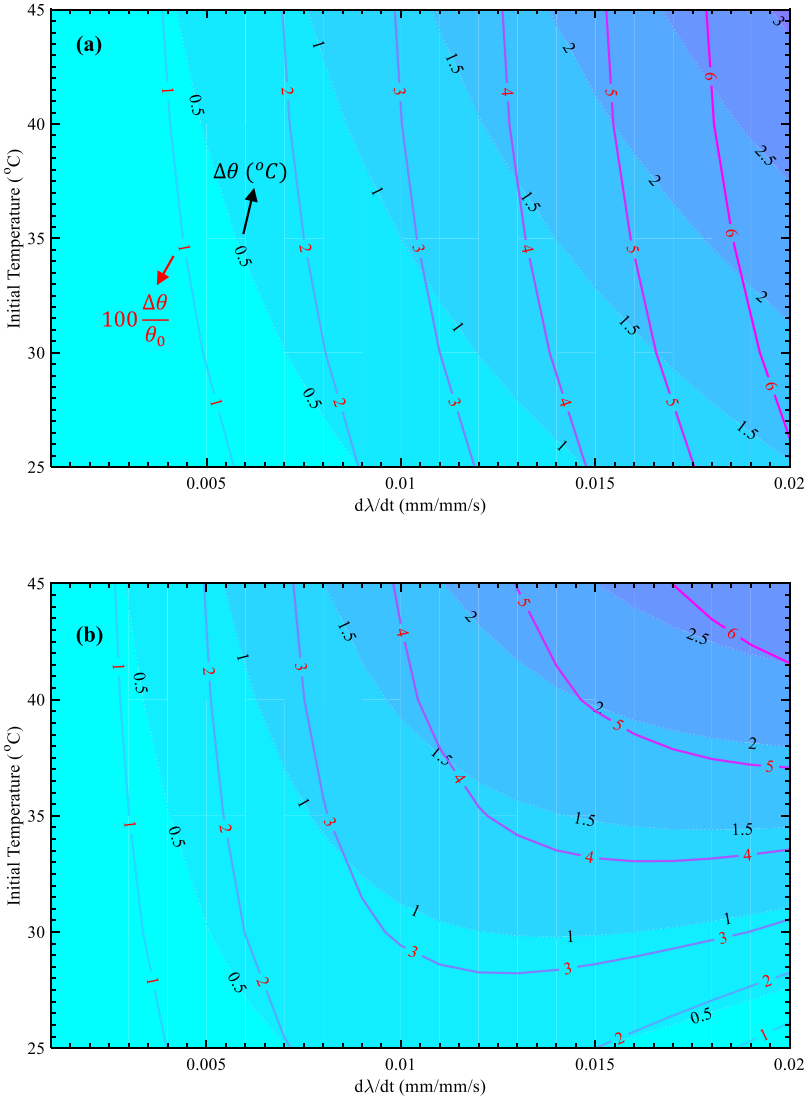

Fig. 9. Initial temperature–strain rate map with isochronous temperature evaluation ($\Delta\theta$) and error ($100\frac{\Delta\theta}{\theta_0}$) contours for loading directions of (a) normal and (b) parallel to the fibers at $\lambda = 1.25$.

The uniaxial elastic stress can be calculated employing equation (A.2) and using Eqs. (31), (46) and (47) for matrix and (A.1), (31), (50) and (52) for fiber:

$$\bar{\mathbf{S}}^{\mathrm{m}}_{\mathcal{E}} = \left(1-\xi^{\mathrm{m}}\right)\mu\left(\theta\right)\left[\left(\lambda^{\mathrm{m}}_{\mathcal{E}}\right)^{\alpha-2} - 2\left(\lambda^{\mathrm{m}}_{\mathcal{E}}\right)^{-\frac{\alpha}{2}-2}\right] \tag{A.3}$$

$$\bar{\mathbf{S}}^{\mathrm{f}}_{\mathcal{E}} = \begin{cases} \dfrac{2\mathrm{k}_1\left(\theta\right)}{\mathrm{J}_{\mathrm{M}}^{\frac{2}{3}}}\left(\mathrm{I}^{*\mathrm{f}}_{4,\mathcal{E}}-1\right)\left[\mathrm{e}^{\mathrm{k}_2\left(\mathrm{I}^{*\mathrm{f}}_{4,\mathcal{E}}-1\right)^2}-1\right]\mathrm{dev}\left(\boldsymbol{a}_0\otimes\boldsymbol{a}_0\right) & \text{if } \mathrm{I}^{*\mathrm{f}}_{4,\mathcal{E}}>0 \\ 0 & \text{otherwise} \end{cases} \tag{A.4}$$

The uniaxial viscous stress can be calculated employing equations (32) and (A.2) and also using Eqs. (48) and (49) for matrix and (51) and (53) for fiber.

References

[1] K.F. Chu, D.E. Dupuy, Thermal ablation of tumours: biological mechanisms and advances in therapy, Nature Rev. Cancer 14 (3) (2014) 199, http://dx.doi.org/10.1038/nrc3672.

[2] R.D. Issels, L.H. Lindner, J. Verweij, P. Wust, P. Reichardt, B.C. Schem, S. Abdel-Rahman, S. Daugaard, C. Salat, C.M. Wendtner, Z. Vujaskovic, Neo-adjuvant chemotherapy alone or with regional hyperthermia for localised high-risk soft-tissue sarcoma: a randomised phase 3 multicentre study, Lancet Oncol. 11 (6) (2010) 561–570, http://dx.doi.org/10.1016/S1470-2045(10)70071-1.

[3] T. Ibelli, S. Templeton, N. Levi-Polyachenko, Progress on utilizing hyperthermia for mitigating bacterial infections, Int. J. Hyperth. 34 (2) (2018) 144–156, http://dx.doi.org/10.1080/02656736.2017.1369173.

[4] S. Zschaeck, P. Wust, I. Melcher, J. Nadobny, D. Rau, J. Striefler, S. Pahl, A. Flörcken, A. Kunitz, P. Ghadjar, Neoadjuvant chemotherapy plus radiation versus chemotherapy plus regional hyperthermia in high-grade soft tissue sarcomas: a retrospective comparison, Int. J. Hyperth. 35 (1) (2019) 314–322, http://dx.doi.org/10.1080/02656736.2018.1498137.

[5] L.H. Lindner, R.D. Issels, Hyperthermia in soft tissue sarcoma, Curr. Treat. Options Oncol. 12 (1) (2011) 12–20, http://dx.doi.org/10.1007/s11864-011-0144-6.

[6] B. Emami, C.W. Song, Physiological mechanisms in hyperthermia: a review, Int. J. Radiat. Oncol. Biol. Phys. 10 (2) (1984) 289–295, http://dx.doi.org/10.1016/0360-3016(84)90015-4.

[7] H.C. Huang, K. Rege, J.J. Heys, Spatiotemporal temperature distribution and cancer cell death in response to extracellular hyperthermia induced by gold nanorods, ACS Nano 4 (5) (2010) 2892–2900, http://dx.doi.org/10.1021/nn901884d.

[8] F.K. Storm, W.H. Harrison, R.S. Elliott, D.L. Morton, Normal tissue and solid tumor effects of hyperthermia in animal models and clinical trials, Cancer Res. 39 (1979) 2245–2251.

[9] R.W. Ogden, Large deformation isotropic elasticity–on the correlation of theory and experiment for incompressible rubberlike solids, Proc. R. Soc. Lond. Ser. A Math. Phys. Eng. Sci. 326 (1567) (1972) 565–584, http://dx.doi.org/10.1098/rspa.1972.0026.

[10] T. Kaster, I. Sack, A. Samani, Measurement of the hyperelastic properties of ex vivo brain tissue slices, J. Biomech. 44 (6) (2011) 1158–1163, http://dx.doi.org/10.1016/j.jbiomech.2011.01.019.

[11] N. Elyasi, K.K. Taheri, K. Narooei, A.K. Taheri, A study of hyperelastic models for predicting the mechanical behavior of extensor apparatus, Biomech. Model. Mechanobiol. 16 (3) (2017) 1077–1093, http://dx.doi.org/10.1007/s10237-017-0874-x.

[12] V. Agrawal, S.A. Kollimada, A.G. Byju, N. Gundiah, Regional variations in the nonlinearity and anisotropy of bovine aortic elastin, Biomech. Model. Mechanobiol. 12 (6) (2013) 1181–1194, http://dx.doi.org/10.1007/s10237-013-0474-3.

[13] M. Destrade, J. Murphy, G. Saccomandi, Rivlin's legacy in continuum mechanics and applied mathematics, Phil. Trans. R. Soc. A 377 (2144) (2019) 20190090, http://dx.doi.org/10.1098/rsta.2019.0090.

[14] T.C. Gasser, R.W. Ogden, G.A. Holzapfel, Hyperelastic modelling of arterial layers with distributed collagen fibre orientations, J. R. Soc. Interface 3 (6) (2005) 15–35, http://dx.doi.org/10.1098/rsif.2005.0073.

[15] K. Li, R.W. Ogden, G.A. Holzapfel, Modeling fibrous biological tissues with a general invariant that excludes compressed fibers, J. Mech. Phys. Solids 110 (2018) 38–53, http://dx.doi.org/10.1016/j.jmps.2017.09.005.

[16] G.A. Holzapfel, T.C. Gasser, R.W. Ogden, W. Ehlers, B. Markert, Comparison of a structural model with a fung-type model using a carotid artery: issues of material stability, in: Proceedings of the 1st GAMM Seminar on Continuum Biomechanics, 2005, pp. 79–89.

[17] M.N. Bajuri, H. Isaksson, P. Eliasson, M.S. Thompson, A hyperelastic fibre-reinforced continuum model of healing tendons with distributed collagen fibre orientations, Biomech. Model. Mechanobiol. 15 (6) (2016) 1457–1466, http://dx.doi.org/10.1007/s10237-016-0774-5.

[18] T.A. Carniel, E.A. Fancello, A transversely isotropic coupled hyperelastic model for the mechanical behavior of tendons, J. Biomech. 54 (2017) 49–57, http://dx.doi.org/10.1016/j.jbiomech.2017.01.042.

[19] H. Huang, W. Tang, Q. Tan, B. Yan, Development and parameter identification of a visco-hyperelastic model for the periodontal ligament, J. Mech. Behav. Biomed. Mater. 68 (2017) 210–215, http://dx.doi.org/10.1016/j.jmbbm.2017.01.035.

[20] A.E. Forte, S. Galvan, D. Dini, Models and tissue mimics for brain shift simulations, Biomech. Model. Mechanobiol. 17 (1) (2018) 249–261, http://dx.doi.org/10.1007/s10237-017-0958-7.

[21] A. Bijalwan, B.P. Patel, M. Marieswaran, D. Kalyanasundaram, Volumetric locking free 3D finite element for modelling of anisotropic visco-hyperelastic behaviour of anterior cruciate ligament, J. Biomech. 73 (2018) 1–8, http://dx.doi.org/10.1016/j.jbiomech.2018.03.016.

[22] A. Karkhaneh Yousefi, M.A. Nazari, P. Perrier, M.S. Panahi, Y. Payan, A visco-hyperelastic constitutive model and its application in bovine tongue tissue, J. Biomech. 71 (2018) 190–198, http://dx.doi.org/10.1016/j.jbiomech.2018.02.008.

[23] S.A. Yousefsani, F. Farahmand, A. Shamloo, A three-dimensional micromechanical model of brain white matter with histology-informed probabilistic distribution of axonal fibers, J. Mech. Behav. Biomed. Mater. 88 (2018) 288–295, http://dx.doi.org/10.1016/j.jmbbm.2018.08.042.

[24] H. Liu, G.A. Holzapfel, B.H. Skallerud, V. Prot, Anisotropic finite strain viscoelasticity: Constitutive modeling and finite element implementation, J. Mech. Phys. Solids 124 (2019) 172–188, http://dx.doi.org/10.1016/j.jmps.2018.09.014.

[25] Y.T. Lu, H.X. Zhu, S. Richmond, J. Middleton, A visco-hyperelastic model for skeletal muscle tissue under high strain rates, J. Biomech. 43 (13) (2010) 2629–2632, http://dx.doi.org/10.1016/j.jbiomech.2010.05.030.

[26] S. Budday, G. Sommer, G.A. Holzapfel, P. Steinmann, E. Kuhl, Viscoelastic parameter identification of human brain tissue, J. Mech. Behav. Biomed. Mater. 74 (2017) 463–476, http://dx.doi.org/10.1016/j.jmbbm.2017.07.014.

[27] Y.L. Liu, G.Y. Li, P. He, Z.Q. Mao, Y. Cao, Temperature-dependent elastic properties of brain tissues measured with the shear wave elastography method, J. Mech. Behav. Biomed. Mater. 65 (2017) 652–656, http://dx.doi.org/10.1016/j.jmbbm.2016.09.026.

[28] M.Z. Kiss, M.J. Daniels, T. Varghese, Investigation of temperature-dependent viscoelastic properties of thermal lesions in ex vivo animal liver tissue, J. Biomech. 42 (8) (2009) 959–966, http://dx.doi.org/10.1016/j.jbiomech.2009.03.002.

[29] B. Zhou, F. Xu, C.Q. Chen, T.J. Lu, Strain rate sensitivity of skin tissue under thermomechanical loading, Phil. Trans. R. Soc. A 368 (1912) (2010) 679–690, http://dx.doi.org/10.1098/rsta.2009.0238.

[30] N. Jalal, M. Zidi, Effect of cryopreservation at -80 °C on visco-hyperelastic properties of skeletal muscle tissue, J. Mech. Behav. Biomed. Mater. 77 (2018) 572–577, http://dx.doi.org/10.1016/j.jmbbm.2017.10.006.

[31] R. Behrou, H. Foroughi, F. Haghpanah, Numerical study of temperature effects on the poro-viscoelastic behavior of articular cartilage, J. Mech. Behav. Biomed. Mater. 78 (2018) 214–223, http://dx.doi.org/10.1016/j.jmbbm.2017.11.023.

[32] D. Garcia-Gonzalez, A. Jérusalem, S. Garzon-Hernandez, R. Zaera, A. Arias, A continuum mechanics constitutive framework for transverse isotropic soft tissues, J. Mech. Phys. Solids 112 (2018) 209–224, http://dx.doi.org/10.1016/j.jmps.2017.12.001.

[33] C. Miehe, Entropic thermoelasticity at finite strains. Aspects of the formulation and numerical implementation, Comput. Methods Appl. Mech. Engrg. 120 (3–4) (1995) 243–269, http://dx.doi.org/10.1016/0045-7825(94)00057-T.

[34] G.A. Holzapfel, J.C. Simo, Entropy elasticity of isotropic rubber-like solids at finite strains, Comput. Methods Appl. Mech. Eng. 132 (1–2) (1996) 17–44, http://dx.doi.org/10.1016/0045-7825(96)01001-8.

[35] J.C. Simo, On a fully three-dimensional finite-strain viscoelastic damage model: formulation and computational aspects, Comput. Methods Appl. Mech. Engrg. 60 (2) (1987) 153–173, http://dx.doi.org/10.1016/0045-7825(87)90107-1.

[36] T.D. Nguyen, H.J. Qi, F. Castro, K.N. Long, A thermoviscoelastic model for amorphous shape memory polymers: incorporating structural and stress relaxation, J. Mech. Phys. Solids 56 (9) (2008) 2792–2814, http://dx.doi.org/10.1016/j.jmps.2008.04.007.

[37] C.O. Rodas, F. Zaïri, M. Naït-Abdelaziz, A finite strain thermo-viscoelastic constitutive model to describe the self-heating in elastomeric materials during low-cycle fatigue, J. Mech. Phys. Solids 64 (2014) 396–410, http://dx.doi.org/10.1016/j.jmps.2013.10.010.

[38] G.A. Holzapfel, B. Fereidoonnezhad, Modeling of damage in soft biological tissues, in: Biomechanics of Living Organs, Academic Press, 2017, pp. 101–123, http://dx.doi.org/10.1016/B978-0-12-804009-6.00005-5.

[39] W. Li, Damage models for soft tissues: a survey, J. Med. Biol. Eng. 36 (3) (2016) 285–307, http://dx.doi.org/10.1007/s40846-016-0132-1.

[40] L. Vujosevic, V.A. Lubarda, Finite-strain thermoelasticity based on multiplicative decomposition of deformation gradient, Theor. Appl. Mech. 28 (29) (2002) 379–399, http://dx.doi.org/10.2298/tam0229379v.

[41] V.A. Lubarda, Constitutive theories based on the multiplicative decomposition of deformation gradient: Thermoelasticity, elastoplasticity, and biomechanics, Appl. Mech. Rev. 57 (2) (2004) 95–108, http://dx.doi.org/10.1115/1.1591000.

[42] M. Vaz Jr., P.A. Muñoz Rojas, M.R. Lange, Damage evolution and thermal coupled effects in inelastic solids, Int. J. Mech. Sci. 53 (5) (2011) 387–398, http://dx.doi.org/10.1016/j.ijmecsci.2011.03.001.

[43] E. Mase, G. Mase, Continuum Mechanics for Engineers, CRC Press LLC, 1999.

[44] G.A. Holzapfel, Nonlinear solid mechanics: a continuum approach for engineering science, Meccanica 37 (4) (2002) 489–490, http://dx.doi.org/10.1023/A:1020843529530.

[45] C. Truesdell, W. Noll, The non-linear field theories of mechanics, in: The Non-Linear Field Theories of Mechanics, Springer, Berlin, Heidelberg, 2004, pp. 1–579, http://dx.doi.org/10.1007/978-3-662-10388-3_1.

[46] D.P. Pioletti, L.R. Rakotomanana, J.F. Benvenuti, P.F. Leyvraz, Viscoelastic constitutive law in large deformations: application to human knee ligaments and tendons, J. Biomech. 31 (8) (1998) 753–757, http://dx.doi.org/10.1016/S0021-9290(98)00077-3.

[47] S.C.H. Lu, K.S. Pister, Decomposition of deformation and representation of the free energy function for isotropic thermoelastic solids, Int. J. Solids Struct. 11 (7–8) (1975) 927–934, http://dx.doi.org/10.1016/0020-7683(75)90015-3.

[48] K.Y. Volokh, Hyperelasticity with softening for modeling materials failure, J. Mech. Phys. Solids 55 (10) (2007) 2237–2264, http://dx.doi.org/10.1016/j.jmps.2007.02.012.

[49] B.D. Coleman, W. Noll, The thermodynamics of elastic materials with heat conduction and viscosity, Arch. Ration. Mech. Anal. 13 (1) (1963) 167–178, http://dx.doi.org/10.1007/BF01262690.

[50] M.A. Zulliger, P. Fridez, K. Hayashi, N. Stergiopulos, A strain energy function for arteries accounting for wall composition and structure, J. Biomech. 37 (7) (2004) 989–1000, http://dx.doi.org/10.1016/j.jbiomech.2003.11.026.

[51] G. Limbert, J. Middleton, A transversely isotropic viscohyperelastic material: application to the modeling of biological soft connective tissues, Int. J. Solids Struct. 41 (15) (2004) 4237–4260, http://dx.doi.org/10.1016/j.ijsolstr.2004.02.057.

[52] J.M. Vassoler, L. Stainier, E.A. Fancello, A variational framework for fiber-reinforced viscoelastic soft tissues including damage, Internat. J. Numer. Methods Engrg. 108 (8) (2016) 865–884, http://dx.doi.org/10.1002/nme.5236.

[53] H. Topol, K. Gou, H. Demirkoparan, T.J. Pence, Hyperelastic modeling of the combined effects of tissue swelling and deformation-related collagen renewal in fibrous soft tissue, Biomech. Model. Mechanobiol. 17 (6) (2018) 1543–1567, http://dx.doi.org/10.1007/s10237-018-1043-6.

[54] C. Whitford, N.V. Movchan, H. Studer, A. Elsheikh, A viscoelastic anisotropic hyperelastic constitutive model of the human cornea, Biomech. Model. Mechanobiol. 17 (1) (2018) 19–29, http://dx.doi.org/10.1007/s10237-017-0942-2.

[55] M. Kazempour, M. Baniassadi, H. Shahsavari, Y. Remond, M. Baghani, Homogenization of heterogeneous brain tissue under quasi-static loading: a visco-hyperelastic model of a 3D RVE, Biomech. Model. Mechanobiol. (2019) 1–3, http://dx.doi.org/10.1007/s10237-019-01124-6.

[56] P.J. Arnoux, P. Chabrand, M. Jean, J. Bonnoit, A visco-hyperelastic model with damage for the knee ligaments under dynamic constraints, Comput. Methods Biomech. Biomed. Eng. 5 (2) (2002) 167–174, http://dx.doi.org/10.1080/10255840290010283.

[57] L. Laiarinandrasana, R. Piques, A. Robisson, Visco-hyperelastic model with internal state variable coupled with discontinuous damage concept under total Lagrangian formulation, Int. J. Plast. 19 (7) (2003) 977–1000, http://dx.doi.org/10.1016/S0749-6419(02)00089-X.

[58] M. Takaza, K.M. Moerman, J. Gindre, G. Lyons, C.K. Simms, The anisotropic mechanical behaviour of passive skeletal muscle tissue subjected to large tensile strain, J. Mech. Behav. Biomed. Mater. 17 (2013) 209–220, http://dx.doi.org/10.1016/j.jmbbm.2012.09.001.

[59] R.W. Ogden, G. Saccomandi, I. Sgura, Fitting hyperelastic models to experimental data, Comput. Mech. 34 (6) (2004) 484–502, http://dx.doi.org/10.1007/s00466-004-0593-y.

[60] J.S. Bergström, M.C. Boyce, Constitutive modeling of the large strain time-dependent behavior of elastomers, J. Mech. Phys. Solids 46 (5) (1998) 931–954, http://dx.doi.org/10.1016/S0022-5096(97)00075-6.

[61] J.S. Bergström, M.C. Boyce, Constitutive modeling of the time-dependent and cyclic loading of elastomers and application to soft biological tissues, Mech. Mater. 33 (9) (2001) 523–530, http://dx.doi.org/10.1016/S0167-6636(01)00070-9.

[62] J.S. Bergstrom, Mechanics of Solid Polymers: Theory and Computational Modeling, William Andrew, 2015, http://dx.doi.org/10.1016/C2013-0-15493-1.

[63] E. Peña, Damage functions of the internal variables for soft biological fibred tissues, Mech. Res. Commun. 38 (8) (2011) 610–615, http://dx.doi.org/10.1016/j.mechrescom.2011.09.002.

[64] J.W. Ju, On energy-based coupled elastoplastic damage theories: constitutive modeling and computational aspects, Int. J. Solids Struct. 25 (7) (1989) 803–833, http://dx.doi.org/10.1016/0020-7683(89)90015-2.

[65] E. Peña, A rate dependent directional damage model for fibred materials: application to soft biological tissues, Comput. Mech. 48 (4) (2011) 407–420, http://dx.doi.org/10.1007/s00466-011-0594-5.

[66] J.R. Dormand, P.J. Prince, A family of embedded runge–kutta formulae, J. Comput. Appl. Math. 6 (1) (1980) 19–26, http://dx.doi.org/10.1016/0771-050X(80)90013-3.

[67] L.F. Shampine, J. Kierzenka, M.W. Reichelt, Solving boundary value problems for ordinary differential equations in MATLAB with bvp4c, Tutor. Notes 2000 (2000) 1–27.

[68] J.D. Leitman, Thermal Conductivity of Meats, (Doctoral dissertation), Georgia Institute of Technology, 1967.

[69] W. Wang, A. Mandelis, Thermally enhanced signal strength and SNR improvement of photoacoustic radar module, Biomed. Opt. Express 5 (8) (2014) 2785–2790, http://dx.doi.org/10.1364/BOE.5.002785.

[70] A. Chawla, S. Mukherjee, B. Karthikeyan, Characterization of human passive muscles for impact loads using genetic algorithm and inverse finite element methods, Biomech. Model. Mechanobiol. 8 (1) (2009) 67–76, http://dx.doi.org/10.1007/s10237-008-0121-6.

[71] S. Kavitha, K.K. Thyagharajan, Efficient DWT-based fusion techniques using genetic algorithm for optimal parameter estimation, Soft Comput. 21 (12) (2017) 3307–3316, http://dx.doi.org/10.1007/s00500-015-2009-6.

[72] M. Ghasemi, D.R. Nolan, C. Lally, An investigation into the role of different constituents in damage accumulation in arterial tissue and constitutive model development, Biomech. Model. Mechanobiol. 17 (6) (2018) 1757–1769, http://dx.doi.org/10.1007/s10237-018-1054-3.

[73] R.L. Haupt, S.E. Haupt, Practical Genetic Algorithms, John Wiley & Sons, 2004.

[74] C. Van Sligtenhorst, D.S. Cronin, G.W. Brodland, High strain rate compressive properties of bovine muscle tissue determined using a split Hopkinson bar apparatus, J. Biomech. 39 (10) (2006) 1852–1858, http://dx.doi.org/10.1016/j.jbiomech.2005.05.015.

[75] L.L. Gras, S. Laporte, D. Mitton, N. Crevier-Denoix, P. Viot, Tensile tests on a muscle: influence of experimental conditions and of velocity on its passive response, in: Proceedings International Research Council on Biomechanical Injuries, Dublin, Ireland (IRC-12-61), 2012, pp. 515–552.